

RESEARCH ARTICLE

10.1002/2014JE004638

Key Points:

- Impacts cause structural and related spectroscopic change in minerals
- Structural deformation differs among parts of the smectite structure
- Impact-induced change may explain contradictory Martian remote sensing results

Correspondence to:

L. R. Friedlander,
lonia.friedlander@stonybrook.edu

Citation:

Friedlander, L. R., T. D. Glotch, D. L. Bish, M. D. Dyar, T. G. Sharp, E. C. Sklute, and J. R. Michalski (2015), Structural and spectroscopic changes to natural nontronite induced by experimental impacts between 10 and 40 GPa, *J. Geophys. Res. Planets*, 120, doi:10.1002/2014JE004638.

Received 18 MAR 2014

Accepted 17 MAR 2015

Accepted article online 23 MAR 2015

Structural and spectroscopic changes to natural nontronite induced by experimental impacts between 10 and 40 GPa

Lonia R. Friedlander¹, Timothy D. Glotch¹, David L. Bish², M. Darby Dyar³, Thomas G. Sharp⁴, Elizabeth C. Sklute¹, and Joseph R. Michalski⁵

¹Geosciences Department, Stony Brook University, Stony Brook, New York, USA, ²Department of Geological Sciences, Indiana University, Bloomington, Indiana, USA, ³Department of Astronomy, Mount Holyoke College, South Hadley, Massachusetts, USA, ⁴School of Earth and Space Exploration, Arizona State University, Tempe, Arizona, USA, ⁵Planetary Science Institute, Tucson, Arizona, USA

Abstract Many phyllosilicate deposits remotely detected on Mars occur within bombarded terrains. Shock metamorphism from meteor impacts alters mineral structures, producing changed mineral spectra. Thus, impacts have likely affected the spectra of remotely sensed Martian phyllosilicates. We present spectral analysis results for a natural nontronite sample before and after laboratory-generated impacts over five peak pressures between 10 and 40 GPa. We conducted a suite of spectroscopic analyses to characterize the sample's impact-induced structural and spectral changes. Nontronite becomes increasingly disordered with increasing peak impact pressure. Every infrared spectroscopic technique used showed evidence of structural changes at shock pressures above ~25 GPa. Reflectance spectroscopy in the visible near-infrared region is primarily sensitive to the vibrations of metal–OH and interlayer H₂O groups in the nontronite octahedral sheet. Midinfrared (MIR) spectroscopic techniques are sensitive to the vibrations of silicon and oxygen in the nontronite tetrahedral sheet. Because the tetrahedral and octahedral sheets of nontronite deform differently, impact-driven structural deformation may contribute to differences in phyllosilicate detection between remote sensing techniques sensitive to different parts of the nontronite structure. Observed spectroscopic changes also indicated that the sample's octahedral and tetrahedral sheets were structurally deformed but not completely dehydroxylated. This finding is an important distinction from previous studies of thermally altered phyllosilicates in which dehydroxylation follows dehydration in a stepwise progression preceding structural deformation. Impact alteration may thus complicate mineral-specific identifications based on the location of OH-group bands in remotely detected spectra. This is a key implication for Martian remote sensing arising from our results.

1. Introduction

Phyllosilicates on the Martian surface have been identified in early-to-mid Noachian terrains primarily by visible near-infrared (VNIR) reflectance spectroscopy [Bibring *et al.*, 2005, 2006; Poulet *et al.*, 2005; Mustard *et al.*, 2008; Ehlmann *et al.*, 2009; Wray *et al.*, 2009]. The occurrence of phyllosilicates in old, heavily bombarded terrains [Mangold *et al.*, 2007; Michalski and Dobreá, 2007; Poulet *et al.*, 2008, 2009; Ehlmann *et al.*, 2009; Fairén *et al.*, 2010] suggests that clay minerals on the Martian surface may have experienced shock metamorphism. Shock metamorphism affects the crystal structures of minerals, and thus their spectra [Johnson *et al.*, 2002, 2007; Johnson and Hörz, 2003; Butler and Frost, 2006; Wright *et al.*, 2006], which may explain the ambiguous phyllosilicate identifications on Mars from midinfrared (MIR) remote sensing data [Friedlander *et al.*, 2012; Sharp *et al.*, 2012].

Recent laboratory work confirms that experimental impacts disrupt MIR phyllosilicate spectra, whereas characteristic smectite VNIR spectral features are retained [Gavin *et al.*, 2013]. Previous experiments also demonstrated that thermal alteration causes spectral changes for both phyllosilicates and zeolites, primarily through the processes of dehydration and dehydroxylation [Che *et al.*, 2011; Che and Glotch, 2012]. Loizeau *et al.* [2007] hypothesized that dehydration or dehydroxylation may be responsible for the apparent lack of phyllosilicates in one bright outcrop in the western part of Mawrth Vallis. Thus, elevated temperatures or shock metamorphism may affect the interpretation of remote sensing data from the Martian surface. Indeed, it has been demonstrated by laboratory spectroscopy and modeling that preexisting phyllosilicates can

Table 1. Analysis Techniques Used to Investigate the Effects of Experimental Impacts on Nontronite Structure and Spectroscopy and Their Comparable Remote and In Situ Sensing Instruments for Mars^a

Analysis Technique	Wavelength Region	Scale	Sensitive to ...	Similar to Remote Sensing Instrument? Y/N (Instrument Name)
Raman spectroscopy	100–1100 cm ⁻¹ (100–9 μm), 785 nm laser (preimpact), 532 nm (after)	Atomic	Changes in polarizability, cationic environments	N, but proposed
VNIR reflectance spectroscopy	0.50–2.50 μm (20,000–4,000 cm ⁻¹)	Combined atomic and bulk	Changes in color, hydration state, cation oxidation state or environment, and NIR OH and H ₂ O overtones	Y, OMEGA, CRISM
MIR emissivity spectroscopy	1300–200 cm ⁻¹ (8–50.0 μm)	Combined atomic and bulk	Si–O bending and stretching fundamental vibrations	Y, TES, THEMIS
MIR ATR spectroscopy	4000–500 cm ⁻¹ (2.50–20.0 μm)	Combined atomic and bulk	OH and H ₂ O fundamental stretching and bending vibrations, metal–OH fundamental stretches and deformations, and Si–O stretch fundamental	N, approximates transmission, good comparison for MIR emissivity results
Mössbauer spectroscopy	N/A (beam energy or counting rate in mm/s)	Nuclear to atomic	Changes in Fe oxidation state, structural environment	Y, MER Mössbauer spectrometer
TEM	N/A (imaging)	Crystal	Imaging impact-induced deformational features	N
XRD	N/A (counts)	Crystal and bulk identification	Amorphization, changes in the crystal lattice, and mineral identification	Y, <i>Curiosity</i> ChemMin instrument

^aCommonly used vibrational units are shown; alternative units are listed parenthetically.

survive postimpact exhumation temperatures [Fairén *et al.*, 2010], but not without minor thermal alteration, and near-infrared (NIR) spectral features from Toro crater ejecta have been found to be consistent with thermally treated nontronite [Gavin and Chevrier, 2010]. In addition, a unique spectral feature centered at 450 cm⁻¹ in Mars Global Surveyor Thermal Emission Spectrometer (TES) data and associated with the detections by the Mars Express/Observatoire pour la Minéralogie, l'Eau, les Glaces et l'Activité (OMEGA) VNIR imaging spectrometer of nontronite-rich deposits around Nili Fossae [Michalski *et al.*, 2010], has been shown to be consistent with nontronite after thermal alteration to 400°C [Che and Glotch, 2014]. A detailed examination of the effects of shock metamorphism on clay mineral spectroscopy may thus provide valuable insights for the analysis and interpretation of Martian remote sensing data.

Due to the abundance of nontronite and nontronite-like smectite identifications on the Martian surface [Bibring *et al.*, 2005, 2006; Poulet *et al.*, 2005, 2008; Loizeau *et al.*, 2007; Mustard *et al.*, 2008; Mckeown *et al.*, 2009; Carter *et al.*, 2013], we focus here on the spectroscopic effects of experimental impacts on a natural nontronite sample (NAU-1, Clay Minerals Society Source Clay). This work builds on that of Gavin *et al.* [2013], providing spectroscopic analyses for one clay mineral over a range of impact pressures, using many laboratory and spectral analysis techniques. It also complements the broad spectroscopic analyses performed on thermally altered phyllosilicate and zeolite samples in Che *et al.* [2011] and Che and Glotch [2012].

The use of multiple spectroscopic techniques allowed us to directly investigate the effects of shock pressure on the structure of clay minerals by comparing results from techniques that are sensitive to changes in different parts of the nontronite structure (Table 1). In particular, spectroscopic techniques in the MIR wavelength region, such as emissivity and attenuated total reflectance (ATR) spectroscopy, are sensitive to the Si–O bending and stretching vibrations of the nontronite tetrahedral sheet [Huang *et al.*, 1999; Bougeard *et al.*, 2000; Bishop *et al.*, 2002a; Palin and Dove, 2004; Michalski *et al.*, 2006], while techniques like VNIR reflectance spectroscopy are sensitive to the overtones and combination bands of metal–OH bonds in the octahedral sheet [Bishop *et al.*, 1999, 2002a, 2002b, 2008; Frost and Klopogge, 2000; Petit *et al.*, 2002, 2004; Neumann *et al.*, 2011]. The extended visible region (0.3–1.0 μm) measures Fe³⁺ crystal-field, electronic transitions that reflect the Fe bonding environment in the octahedral sheet and can be compared to Mössbauer spectroscopic results [Burns, 1993; Dyar *et al.*, 2008]. Thus, by comparing the effects of impacts on the spectral signatures detected by all of these techniques, we can begin to investigate the complex structural changes

produced in nontronite by impact alteration. These related structural and spectroscopic effects have important implications for the analysis of remote sensing results from the Martian surface and may help explain the differences between ambiguous MIR phyllosilicate detections and definitive VNIR detections.

2. Background

2.1. Phyllosilicate Identifications on Mars

2.1.1. Orbital Identifications

In contrast to the detailed and unambiguous identifications of phyllosilicates on the Martian surface from VNIR reflectance spectra [Bibring *et al.*, 2005, 2006; Poulet *et al.*, 2005; Bishop *et al.*, 2008; Ehlmann *et al.*, 2008, 2009; Mustard *et al.*, 2008; Wray *et al.*, 2009], identifications from MIR (5–50 μm) emission spectroscopy have been ambiguous [Bandfield, 2002; Michalski *et al.*, 2006, 2010; Michalski and Fergason, 2008; Mcdowell and Hamilton, 2009], suggesting low abundances of these minerals. These results contradict the apparently high phyllosilicate abundances estimated by nonlinear spectral unmixing [Poulet, 2004; Liu and Glotch, 2014] in regions where strong VNIR absorption features characteristic of phyllosilicates lead to robust identifications [Poulet *et al.*, 2008]. For example, Michalski and Fergason [2008] examined TES data for Mawrth Vallis and could not find phyllosilicate detections from TES spectral index mapping comparable to those from OMEGA and CRISM (Compact Reconnaissance Imaging Spectrometer for Mars) data. However, Al-rich phyllosilicate species (and allophane) have been specifically identified by VNIR reflectance (CRISM) spectroscopy and suggested by TES spectral modeling [Bishop and Rampe, 2014]. This implies that TES phyllosilicate detections at Mawrth Vallis and elsewhere [e.g., Rampe *et al.*, 2012] may somehow be dominated by Al-rich phyllosilicate spectra, even though Mg/Fe-rich smectites are thought to be one of the most abundant phyllosilicate species on Mars based on VNIR reflectance spectroscopy [Carter *et al.*, 2013]. These low-nontronite detections thus remain a mystery, despite recent identifications by TES modeling of specific Al-phyllosilicate species. Our results demonstrate that impacts can alter the spectral signatures of natural phyllosilicates, perhaps providing a mechanism to explain the apparently low abundance of Fe/Mg smectites in TES deconvolution models.

Several hypotheses have been proposed to explain the apparent lack of characteristic phyllosilicate fundamental vibrational bands in MIR spectroscopic data from the Martian surface. Michalski and Fergason [2008] suggested three possible explanations: surface roughness, multiple surface temperatures at subpixel scales, and low absolute mineral abundances combined with spatial sampling differences. Ruff and Hamilton [2009] also suggested that phyllosilicates might be present only at or near the TES detection limit as established by Ruff and Christensen [2007]. Other researchers have found that separating phyllosilicates from other high-silica phases in linear spectral mixture analysis models of TES data at global scales is difficult [Bandfield, 2002; Wyatt and McSween, 2002; Michalski *et al.*, 2005, 2006]. For instance, Bandfield [2002] examined TES data at 1 pixel per degree spatial resolution to determine global mineral distributions, finding a great deal of spectral similarity between phyllosilicates and high-Si glass phases. He also found, however, that certain phyllosilicate species display characteristic vibrational bands in a region of the MIR that is frequently excluded from atmospherically corrected TES spectra. Ruff [2003], however, suggested that recognizing these subtle differences may make MIR phyllosilicate identifications possible at regional to local, rather than global, scales.

Attempts to identify phyllosilicates at regional and local scales using MIR data of the Martian surface have been partially successful. Ruff and Christensen [2007] used two spectral indices to differentiate between smectites and TES Surface Type 2 (ST2), a TES average spectrum from 4 to 7 regional locations on Mars, which was originally interpreted as a basaltic andesite [Bandfield *et al.*, 2000]. They scrutinized the MIR data from regions where phyllosilicate identifications by VNIR reflectance spectroscopy were thought to be unambiguous and found systematic correlations to a spectral index based on long-wavelength phyllosilicate emission features. They did not, however, unambiguously identify phyllosilicates directly using MIR data. More recently, Michalski *et al.* [2010] used VNIR data from OMEGA in combination with TES MIR data to develop a TES spectral index that correlated VNIR reflectance-based phyllosilicate identifications in the Nili Fossae region with spectral signatures from MIR emissivity. However, the TES Nili Fossae phyllosilicate spectra were ambiguous with respect to specific phyllosilicate phases and indicated that phyllosilicates at Nili Fossae were either extremely disordered or were embedded in a matrix of basaltic glass. In later work, Viviano and Moersch [2012] used an approach similar to Michalski *et al.* [2010] to map phyllosilicates with

the Mars Odyssey Thermal Emission Imaging System (THEMIS). However, they convolved THEMIS with OMEGA and CRISM data and also failed to provide unambiguous phyllosilicate detections from the emissivity spectra alone. Thus, MIR emissivity data from the Martian surface have so far offered limited new information to complement robust VNIR identifications, while specific mineral phase identifications directly from MIR spectroscopic data generally remain ambiguous for nontronite-bearing regions. Because impacts are an important geologic process on Mars, they are likely to have played a role in the evolution of Martian phyllosilicate mineralogy. In addition, shock metamorphism can affect both VNIR and MIR spectra [Johnson *et al.*, 2002, 2007]. As a result, the effects of shock on phyllosilicate spectra may partially explain the disconnect between VNIR and MIR phyllosilicate detections from orbital remote sensing data of the Martian surface.

Some recent work using both VNIR and MIR remote sensing techniques has begun to support the hypothesis that Martian phyllosilicates may have been structurally disordered by impacts and that this might be affecting their identifications by different remote sensing techniques. First, CRISM phyllosilicate spectra taken at Toro crater and the VNIR reflectance spectra of nontronite heated to 400°C were shown to be similar by Gavin and Chevrier [2010]. They noted especially that these results implied that the Toro crater phyllosilicates predated the impact event, and thus were at least Noachian in age. This supports the hypothesis that phyllosilicates in Nili Fossae are old and might have been structurally disordered by impacts, rather than generated by them [e.g., Michalski *et al.*, 2010]. More recently, Che and Glotch [2014] directly matched TES phyllosilicate spectra in the Nili Fossae region with the laboratory emissivity spectra of thermally altered nontronite heated to ~400°C using a factor analysis and target transformation (FATT) algorithm [Thomas and Bandfield, 2013]. These results directly support our hypothesis that impact-induced structural disorder may contribute to the ambiguity of phyllosilicate detections by MIR spectroscopic techniques.

2.1.2. Surface Identifications

There is only ambiguous Mössbauer evidence for phyllosilicates on the Martian surface. In their broad summaries of the results from the Mössbauer spectrometers aboard the Mars Exploration Rovers (MERs) *Spirit* and *Opportunity*, Morris *et al.* [2006a, 2006b] did not identify any specific Mössbauer doublets as representing phyllosilicates. However, one of the Fe³⁺ doublets (Fe3D3) in rocks from the Burns Formation was unassigned, with an isomer shift (δ) of 0.37 ± 0.02 mm/s and quadrupole splitting (Δ) of 0.62 ± 0.03 mm/s. Moreover, rocks at both landing sites contain a doublet assigned by Morris *et al.* [2006a, 2006b] to represent nanophase ferric oxide (npOx) with $\delta = 0.38 \pm 0.02$ mm/s and $\Delta = 0.89 \pm 0.02$ mm/s. Intriguingly, these features closely overlap values reported for various clay minerals, for which there is vast Mössbauer literature [e.g., Dyar, 2002; Dyar *et al.*, 2006, 2008]. Consistent with this possibility, Clark *et al.* [2007] presented compelling chemical evidence for the presence of montmorillonite in “independence class” samples from the Columbia Hills and speculate that “smectite is actually present but its mineralogical structure has been masked from detection by the MER instrument suite.” It is possible that the mineral assignments made in these Mössbauer papers may be nonunique, so further comparisons of MER results with clay mineral spectra are warranted.

X-ray diffractometry (XRD) results from the ChemMin instrument aboard the Mars Science Laboratory (MSL) rover *Curiosity* initially failed to directly identify phyllosilicates but did find an X-ray amorphous, Fe-rich phase that hosts a significant amount of soil volatiles in both the Rocknest aeolian bedform [Bish *et al.*, 2013] and its sand shadow [Blake *et al.*, 2013]. More recently, abundant phyllosilicates have been identified by *Curiosity* in the Sheepbed mudstone at Gale Crater [Morris *et al.*, 2014; Rampe *et al.*, 2014; Vaniman *et al.*, 2014]. However, specific identifications of individual phyllosilicate species from these XRD patterns have not been possible [Rampe *et al.*, 2014; Vaniman *et al.*, 2014]. In addition, some of the phyllosilicates identified by *Curiosity* are associated with an X-ray amorphous phase [Morris *et al.*, 2014] whose formation process(es) is (are) not yet well understood. Thus, results from ChemMin confirm the presence of phyllosilicates on the Martian surface, while also leaving open questions about their formation and alteration by later processes including potential impacts.

2.2. Previous Laboratory Studies

2.2.1. Experimental Shock and Shock Metamorphism

During impacts, intense pressure waves pass through geologic material, initiating processes that cause structural modifications and alteration in the affected rocks and minerals, propagating existing defects and increasing structural disorder [Gault and Heitowitz, 1963; Stöffler, 1972, 1974, 1984; Hanss *et al.*, 1978; Lange and Ahrens, 1982; Bischoff and Stöffler, 1992]. Pressure, and associated heating, can also induce transitions to entirely

new mineral phases [Coes, 1953; Stishov and Popova, 1961], which have been identified in naturally and artificially shocked geologic materials [Chao *et al.*, 1960, 1961, 1962; De Carli and Milton, 1965; Stöffler, 1971]. Laboratory shock experiments have contributed to the understanding of shock metamorphism and related processes since impacts were first recognized as important geologic processes [French, 1968; Stöffler, 1974].

In natural samples, determining whether secondary mineral phases resulted from shock or alteration can be difficult [Bruckenthal and Pieters, 1984]. Shock experiments reduce this ambiguity. Laboratory shock experiments also provide important sources of spectroscopic data for remote sensing analysis. In one early set of shock experiments, Adams *et al.* [1979] observed distinct changes in the reflectance spectra of shocked versus unshocked plagioclase, pyroxene, and glass, and they noted the pressures at which these changes occurred. Later researchers, using shock experiments to examine the spectra of different minerals after exposure to the same shock pressures, found that shock effects depend dramatically on the mineral involved. In an investigation of the effects of shock on the MIR emissivity and hemispherical reflectance spectra of feldspar and pyroxene, for example, Johnson *et al.* [2002] found that experimental impacts up to 63 GPa produced fewer spectral changes for pyroxene than for feldspar. Later work by Johnson *et al.* [2007] showed that spectra modeled by multiple end-member spectral mixing algorithms using libraries composed of common mineral and glass spectra replicated the emissivity spectra of shocked basalts reasonably well up to pressures of 20–25 GPa. At higher pressures, their reported model errors increased significantly. However, including spectra from shocked feldspars in the spectral libraries improved fits. Thus, understanding the effects of shock on mineral spectroscopy can help improve remote sensing data interpretation. This may be particularly important for understanding and interpreting Martian phyllosilicate identifications.

2.2.2. Shock Metamorphism of Phyllosilicates and Phyllosilicate Spectroscopy

Relative to the large body of work on the structural and spectroscopic effects of shock on rocks and rock-forming minerals, little work has been published about the effects of impacts on the structure and spectra of phyllosilicate minerals. Early work focused on the effects of shock on the dehydration of phyllosilicates, particularly serpentine [Boslough *et al.*, 1980; Lange and Ahrens, 1982; Tyburczy and Ahrens, 1987]. Using IR absorption spectroscopy, Boslough *et al.* [1980] confirmed the release of bound hydroxyl and H₂O from the structures of serpentine, nontronite, and kernite after experimental impacts. They also connected decreased absorbance for both the OH-group stretching and H₂O hydrogen bond resonances in the postshock spectra of all three minerals to this H₂O loss. Using shock-recovery experiments, Lange and Ahrens [1982] determined the amount of shock-induced structural hydroxyl loss from serpentine as a function of shock pressure between 25 and 45 GPa, and they used IR absorption spectroscopy to confirm these structural changes. Tyburczy and Ahrens [1987] later found that shocked serpentine dehydrates 20 to 30 times faster at Martian surface conditions than unshocked serpentine does, showing that impacts and related processes may have played an important role in the geologic evolution of planetary surfaces and atmospheres.

Shock effects have also been invoked to explain the color of the Martian surface. In particular, Weldon *et al.* [1982] observed that a sample of Riverside nontronite reddened and darkened after experimental impacts between 18 and 30 GPa. Using optical microscopy, X-ray diffractometry, ⁵⁷Fe Mössbauer spectroscopy, and IR spectroscopy, they determined that partial dehydroxylation changed the Fe coordination state and shifted characteristic Fe³⁺/O²⁻ charge transfer features into the visible wavelength region, producing a redder, darker nontronite sample. Weldon *et al.* [1982] attributed their results primarily to impact-induced heating. However, later work by Boslough *et al.* [1986] showed that the effects of shock differed from those of heat. Boslough *et al.* [1986] contrasted the effects produced on a sample of Riverside nontronite by experimental impacts between 7 and 32 GPa with the effects produced by heating the sample in air (annealing) between 400 and 1000°C. They found that both shocked and heated samples of Riverside nontronite showed similar increases in magnetization, but that postshock samples were structurally distinct from annealed samples, as determined by X-ray diffraction. Both processes altered the nontronite sample's color toward redder and darker, thus Boslough *et al.* [1986] suggested that repeated impacts might have altered the properties of nontronite to be consistent with those of the fine dust on the surface of Mars.

Despite the early recognition of their potential importance, detailed laboratory spectroscopic studies of the effects of shock and related processes on phyllosilicates have only recently begun. Initial experiments

focused on the effects of thermal alteration on phyllosilicate and zeolite structures and spectroscopy. *Che et al.* [2011] conducted extensive laboratory work exploring changes in the MIR spectra of phyllosilicate and zeolite minerals after heating. *Che and Glotch* [2012] examined the VNIR spectra of the same thermally altered mineral suite. These and other studies [*Moskowitz and Hargraves*, 1984; *Gavin and Chevrier*, 2010; *Daly et al.*, 2011] showed that heating fundamentally alters phyllosilicate spectra, mostly through dehydration and dehydroxylation. However, as early impact-shock experiments showed, the effects of elevated temperatures differ from the effects of pressure [e.g., *Weldon et al.*, 1982; *Boslough et al.*, 1986]. Thus, additional work to examine shock pressure effects on phyllosilicate spectra is warranted, especially to improve the current understanding of the ways in which impact processes may variably affect the VNIR and MIR spectra of phyllosilicates.

Recent work by *Gavin et al.* [2013] began to address this by providing direct comparisons between preshock and postshock phyllosilicate spectra for individual shock experiments. However, these results cannot be associated with specific pressures, because *Gavin et al.* [2013] reported primarily impactor velocity and modeled impact pressures for only two samples (nontronite and montmorillonite). In contrast, the data presented in this work show the progression of structural change in one natural nontronite sample as a result of experimental impacts at peak pressures from 10 to 40 GPa. These experiments are unvented, which previous work suggests may affect sample devolatilization [*Kraus et al.*, 2013]; although the exact effects of vented versus unvented shock-recovery experimental setups are, as yet, unclear [*Boslough et al.*, 1980; *Kraus et al.*, 2013]. Nonetheless, our work provides additional information about the relationship between pressure and spectroscopically important structural changes in nontronite. In addition to conducting experiments at a range of pressures, we also used an extensive suite of analysis techniques (Table 1) to explore the postimpact structural and spectral changes in nontronite. We selected each of our analysis techniques (Table 1) to be able to examine nontronite's postimpact structural change at various scales (i.e., nuclear, atomic, crystal, and bulk) and with regard to characteristic parts of the nontronite structure (e.g., OH versus Si–O vibrational regions). Based on our results, we offer a hypothesis that may explain the differences between VNIR and MIR phyllosilicate identifications from the remote sensing of Mars.

3. Methodology

We performed our impact experiments at the Flat Plate Accelerator (FPA) at NASA's Johnson Space Center (JSC), which provides unique data on the effects of shock pressure. By attaining peak pressure through the process of shock reverberation, the FPA achieves lower peak temperatures than would occur in natural impacts of comparable pressure [*Gibbons and Ahrens*, 1971]. Because each is sensitive to different parts of the phyllosilicate structure, a variety of spectroscopic and analytical techniques (Table 1) was used to analyze the starting material and impact products: X-ray diffractometry (XRD), Mössbauer spectroscopy, VNIR reflectance spectroscopy, MIR attenuated total reflectance (ATR) spectroscopy, MIR emission spectroscopy, and transmission electron microscopy (TEM). Using these analyses, we describe the postimpact structural changes in phyllosilicates that produce spectral changes. At the FPA, shock pressures are derived from projectile velocity and the shock impedances of the flyer plate and sample assembly, using the Rankine-Hugoniot equations [*Rankine*, 1870; *Hugoniot*, 1889; *Gault and Heitowitz*, 1963]. This provides shock pressure estimates for all of our samples and allows us to associate specific spectral and structural changes with known peak shock pressures.

3.1. Sample Acquisition and Preparation

We purchased our natural nontronite sample (NAu-1) from the Clay Minerals Society Source Clays Repository. The chemical composition of this sample was originally reported in detail by *Keeling et al.* [2000]. To remove impurities occurring mostly in the $>2\ \mu\text{m}$ size fraction [*Moore and Reynolds*, 1989], we ground our sample and separated the $<2\ \mu\text{m}$ size fraction by sieving (to separate the $<45\ \mu\text{m}$ size fraction), followed by settling using centrifugation [*Moore and Reynolds*, 1989]. In this technique, particles $<20\ \mu\text{m}$ are assumed to approximately obey Stoke's Law, and, as a result, centrifugation for various lengths of time controls the size of the particles that settle out of suspension. Smaller particles are retained in the supernatant. The complete process is described in more detail by *Moore and Reynolds* [1989]. We then washed the sample with acetic acid to remove carbonate impurities. NAu-1 nontronite contains an Al-rich contaminant, which has previously been identified as kaolinite and may also provide a source of octahedral

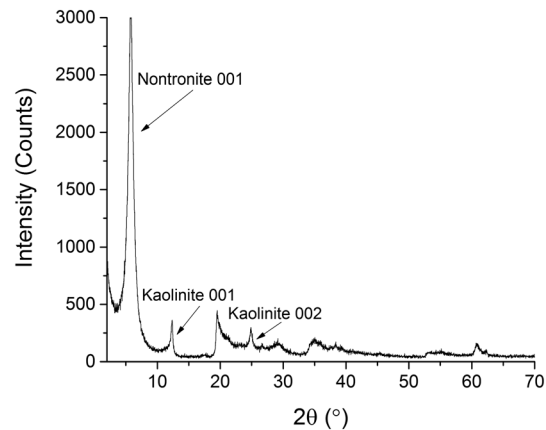


Figure 1. XRD pattern of preimpact, prepared NAU-1 nontronite. The Al-rich contaminant (kaolinite) is identified by characteristic diffraction peaks, our sample contains ~16 wt %, as determined using the reference intensity ratio method [Chung, 1974].

aluminum [Keeling *et al.*, 2000]. Our processed nontronite sample contains ~16 wt % kaolinite, as determined by the reference intensity ratio method [Chung, 1974] from our preimpact XRD analysis (Figure 1).

3.2. Impact Experiments

Impact experiments were conducted using a shock-reverberation setup at NASA's FPA facility at JSC. Sample powders were pressed into pellets and loaded into stainless steel sample containers that were individually milled to match the dimensions of the pellet. Pressed pellets reduce the initial porosity of the sample, reducing the entropy added to the system by pore collapse. On average, 0.15 g of sample was used in each shock experiment. Stainless steel and fansteel flyer plates were used to produce impacts approximating one-dimensional shock [See *et al.*,

2012]. Projectiles were launched horizontally at the mounted sample containers and their velocities were measured directly by lasers in the flight path. Measured impactor velocities ranged from 0.872 km/s (10.2 GPa) to 1.349 km/s (39.1 GPa), just prior to impact. These velocities were converted to pressure by one-dimensional shock-stress calculations after Gault and Heitowitz [1963], giving shock-stress accuracies of $\pm 1\%$. The tilt of the projectile must be less than 3° to approximate one-dimensional shock. Duel cameras stationed along the flight path monitored the projectile tilt. Samples from impacts with tilts great than 3° were not used in our study. We conducted shock experiments at six peak shock pressures between 10 and 40 GPa as follows: 10.2, 19.7, 25.2, 30.6, 34.6, and 39.1 GPa. After successful experiments, sample containers were cut open, enabling recovery of nearly the entire (~15 mg) shocked sample.

3.3. Postimpact Spectroscopic Analysis Technique Selection

Each of the selected techniques was chosen for comparison to existing or proposed Mars remote sensing instruments and for detailed investigation of the many parts of the complex nontronite structure (Table 1). VNIR reflectance spectroscopy probes the Fe-electronic transitions between 0.5 and 1.0 μm (0.65 and 0.92 μm for Fe^{3+} in nontronite) [Burns, 1993; Clark, 1999], metal-OH stretching overtones in combination with both bound H_2O and adsorbed H_2O (1.4 μm) [Bishop *et al.*, 1994, 2002a; Bishop and Pieters, 1995; Petit *et al.*, 1999, 2004], H-O-H structural H_2O bend in combination with adsorbed H_2O vibrations (1.9 μm) [Bishop *et al.*, 1994], and characteristic metal-OH combination and overtone vibrations (2.1–2.3 μm) [Petit *et al.*, 1999; Bishop *et al.*, 2002a]. Most of the identifications of phyllosilicates on the Martian surface from VNIR reflectance remote sensing data are based on characteristic metal-OH combination and overtone bands in the 2.17–2.36 μm wavelength region. The 1.4 and 1.9 μm features are sometimes used in association with these bands to strengthen phyllosilicate identifications [Bibring *et al.*, 2005; Poulet *et al.*, 2005; Mustard *et al.*, 2008]. Laboratory VNIR reflectance data are comparable to OMEGA and CRISM data, making this a good technique for direct comparisons with Martian remote sensing VNIR reflectance data. ATR spectroscopy provides useful information on phyllosilicate structures in the MIR frequency region, 4000–500 cm^{-1} (2.5–20 μm), and can detect changes to the nontronite tetrahedral sheet Si-O bends and stretches (1250–850 cm^{-1}), bands related to structural H_2O and adsorbed H_2O (1630 cm^{-1} and 3500–3100 cm^{-1}), as well as octahedral sheet metal-O bends, Fe-FeOH bends, and Fe- and Al-smectite OH stretches (650 cm^{-1} , 820 cm^{-1} , and >3500 cm^{-1} , respectively) [Frost and Klopogge, 2000; Bishop *et al.*, 2002a, 2002b; Neumann *et al.*, 2011]. Because it spans both the fundamental and overtone regions and jointly provides information on both the octahedral and tetrahedral sheets, ATR spectroscopy is particularly useful for examining structural change in impact-altered nontronite, especially differences in the effects of impacts on various parts of the nontronite structure. Laboratory MIR emissivity spectra are comparable to TES and THEMIS data from the Martian surface and are sensitive to changes in the characteristic Si-O bending (400–550 cm^{-1}) and stretching (~ 1000 cm^{-1}) modes of phyllosilicate minerals, as well as diagnostic

metal–O–Si bends reflective of changes in both the octahedral and tetrahedral sheets in combination ($\sim 500\text{ cm}^{-1}$) [Michalski et al., 2006; Bishop et al., 2008]. Raman spectroscopy is sensitive to even small changes in the bonding environments of crystal structures [Frost, 1995; Huang et al., 1996; Gavin et al., 2009]. A Raman spectrometer will be on the European ExoMars Rover [European Space Agency, 2013] and another Raman spectrometer was recently selected as a fine-scale mineralogical mapping and organic compound detection experiment on board NASA's Mars 2020 mission [Mustard et al., 2013]. XRD data provide information on the long-range structure and crystallographic order of samples, whereas TEM can be used to visually detect impact-induced structures and structural changes at atomic scales. Finally, Mössbauer spectroscopy provides information on the Fe oxidation and electronic states in our samples. Mössbauer results can be compared to the crystal-field transitions detected in the visible wavelength region by VNIR reflectance spectroscopy to investigate changes to the Fe^{3+} cation octahedral sites in nontronite [Burns, 1993; Clark, 1999; Keeling et al., 2000]. VNIR reflectance, ATR, MIR emissivity, and Raman spectra were acquired at the Vibrational Spectroscopy Laboratory at Stony Brook University. XRD data were acquired at Indiana University, TEM data at Arizona State University, and Mössbauer spectra at Mount Holyoke College.

3.3.1. VNIR Reflectance Spectroscopy

We collected VNIR bidirectional reflectance spectra of each sample between 0.35 and $2.5\ \mu\text{m}$ (28571 cm^{-1} – 4000 cm^{-1}) on an Analytical Spectral Devices (ASD) Instruments (now PANalytical) Field Spec 3 Max Spectroradiometer fitted with an 8° field of view foreoptic. This instrument uses three detectors to cover the relevant VNIR wavelength range: a VNIR 512 element silicon diode array for the 0.35 – $1.00\ \mu\text{m}$ wavelength region, one shortwave infrared (SWIR) camera with a thermoelectrically (TE) cooled InGaAs photodiode for the 1.00 – $1.83\ \mu\text{m}$ wavelength region, and a second SWIR camera with another TE cooled InGaAs photodiode for the 1.83 – $2.50\ \mu\text{m}$ wavelength region. As a result, the spectral resolution of the instrument also varies by wavelength region. At $0.70\ \mu\text{m}$, the full width at half maximum (FWHM) spectral resolution is 3 nm , and it is 10 nm at both 1.40 and $2.10\ \mu\text{m}$. For the spectral region 0.35 – $1.00\ \mu\text{m}$, the instrument has a sampling interval of 1.4 nm , and for the region 1.00 – $2.50\ \mu\text{m}$, it has a sampling interval of 2 nm [Analytical Spectral Devices (ASD), 2014]. Both the spectral resolution and sampling intervals of our spectrometer over the 0.35 – $2.50\ \mu\text{m}$ wavelength region are comparable to, and slightly better, than the spectral resolutions of either the CRISM (6.55 nm/channel) or OMEGA (7 nm —VNIR, 20 nm —NIR) Mars remote sensing instruments. We used a white fluorescent light source to illuminate the samples [ASD, 2014]. The reflectance spectra were referenced to an isotropic Spectralon™ calibration target. We used set incidence and emergence angles of $30 \pm 2^\circ$ and 0° , respectively, for all measurements. Samples were held in a matte-black painted sample cup that has no reflectance features in the relevant wavelength region. We conducted all of our VNIR reflectance measurements in a sealed glove bag in the presence of Drierite™ (CaSO_4 and CoCl_2) desiccant grains with continuous (as needed) N_2 -gas inflow to maintain a relative humidity below 15% for the duration of our measurements. Prior to taking these measurements, all of our samples were gently ground using a mortar and pestle and placed in a desiccation cabinet with $\text{RH} = 30\%$ in the presence of a synthetic silica bead desiccant for over 100 h . In this controlled relative humidity environment, without heating the samples, we expect to reduce the effect of adsorbed H_2O on our nontronite spectra without inducing layer collapse [Morris et al., 2009, 2010, 2011]. In addition, we performed a continuum removal (embedded in the ENVI 5.1/IDL 8.3 image processing software package) on all of our laboratory spectra. This process assumes that the reflectance spectrum continuum is a convex hull overlying the spectrum itself and divides this ideal continuum out of the spectrum (Exelis Visual Information Services, Explanation of the ENVI/IDL continuum removal process, <http://www.exelisvis.com/docs/ContinuumRemoval.html>). Continuum removal ensures that individual spectral features are being compared from a common baseline and is a common spectral processing technique for comparing spectral feature transitions between the spectra of multiple samples [Clark, 1999]. We also normalized our spectra to one another using the `norm_spec` command in Davinciwiki (Explanation of the spectrum normalization function, http://davinci.asu.edu/index.php?title=norm_spec), which further ensured that all spectral features were compared from a common baseline. The same processes were also applied to all of the relevant spectral regions analyzed in our band depth comparisons; for the ATR spectra, we first converted absorbance to reflectance ($R = 1/10^{\text{Abs}}$) and then performed our analyses.

3.3.2. MIR ATR Spectroscopy

We collected ATR spectra between 4000 and 500 cm^{-1} on a Nicolet 6700 Fourier transform infrared (FTIR) spectrometer purged of CO_2 and water vapor and equipped with a Smart Orbit single-bounce ATR accessory

with a type-IIA diamond ATR element. The sample is pressed against the ATR element to bring it into intimate optical contact with the diamond. IR radiation passes through the diamond and into the sample where it is totally reflected in the frequency regions over which the sample is nonabsorbing and is transmitted in frequency regions where the sample absorbs. ATR spectra thus have high spectral contrast and strongly resemble transmission spectra, which they approximate for quantitative purposes [Fahrenfort, 1961].

3.3.3. MIR Emission Spectroscopy

Emissivity spectra in the MIR range ($2000\text{--}200\text{ cm}^{-1}$) were collected on a Nicolet 6700 FTIR purged of CO_2 and water vapor, by switching off the attached Globar IR source and measuring the emitted radiation from the heated samples directly. Prior to heating, we pressed the samples into pellets to increase their emissivity contrast and reduce multiple scattering. Heated samples were maintained at $\sim 80^\circ\text{C}$ to provide adequate emissivity signal. Previous work has shown that clay minerals do not fully dehydrate until exposed to temperatures of 100°C or higher and that spectral change does not occur until well above 100°C , as high as 500°C for some phyllosilicate samples [Harris *et al.*, 1992; Fitzgerald *et al.*, 1996; Roch *et al.*, 1998; Rocha, 1999; Carroll *et al.*, 2005; Gavin and Chevrier, 2010; Che *et al.*, 2011; Che and Glotch, 2012]. Therefore, dehydration via heating for emissivity measurements was not a concern. We calibrated our spectra using warm ($\sim 70^\circ\text{C}$) and hot ($\sim 100^\circ\text{C}$) blackbody standards. We used a CsI beamsplitter and DLaTGS detector with a CsI window to acquire all of our emissivity spectra. Spectra were calibrated in the manner of Ruff *et al.* [1997].

3.3.4. Raman Spectroscopy

We used a WITec alpha300R confocal Raman imaging system using both 532 and 785 nm lasers with nominal powers of 50 mW (532 nm laser) and 150 mW (785 nm laser) to collect our Raman spectra. We used the 532 nm laser for our preimpact Raman spectrum but found that after exposure to experimental impacts our samples generated considerable fluorescence under the 532 nm laser. We attempted to reduce this fluorescence and improve our signal/noise through the use of a 785 nm laser, despite the lower signal that this laser produces. Due to the low overall signal/noise of our impact-altered samples, we used a 1200 g/mm grating with a 100X microscope objective, both the highest available on our Raman imaging system. For the laser wavelengths used, this combination gives approximate 700 nm (532 nm laser) and 1008 nm (785 nm laser) spot sizes.

3.3.5. Transmission Electron Microscopy

Samples were prepared for TEM analysis by crushing in clean acetone and dispersing the suspension onto a lacey carbon film support grid. Grids were then dried under a 100 W incandescent light bulb for several minutes before loading into the TEM sample holder. The clay particles were examined using a Philips CM200FEG S/TEM instrument in the LeRoy-Eyring Center for Solid State Science at Arizona State University. Selected area electron diffraction (SAED) patterns were collected for each particle to determine crystallinity and disorder. Bright field images were used to investigate particle size and morphology. High-resolution images of (001) lattice fringes were recorded to investigate thickness and order in the clay crystallites.

3.3.6. X-Ray Diffraction

X-ray powder diffraction analyses were conducted using a Bruker D8 Advance instrument with $\text{CuK}\alpha$ radiation, incident- and diffracted-beam Soller slits, and a SolX energy-dispersive point detector, using a tube power of 45 kV and 35 mA, over a $2\text{--}70^\circ$ range of 2θ with a 0.02° step size. Starting materials were analyzed both as powders mounted in cavities (i.e., random powder mounts) and as oriented deposits on zero-background quartz plates. All shocked products were analyzed only as deposits on zero-background quartz plates, due to the very small amount of sample available. This small amount of available sample led to increased noise in some patterns, especially for impacts at pressures 19.7 GPa and above. All samples were measured in ambient laboratory conditions of approximately 44% relative humidity.

3.3.7. Mössbauer Spectroscopy

Between 7 and 17 mg of each sample (depending on availability) was mixed with sugar under acetone before mounting in a sample holder confined by Kapton® polyimide film tape. Mössbauer spectra were acquired using a source of $\sim 60\text{ mCi } ^{57}\text{Co}$ in Rh on a WEB Research Co. model WT302 spectrometer (Mount Holyoke College) at 295 K. Results were calibrated against a $25\text{ }\mu\text{m } \alpha\text{-Fe}$ foil. Run times were 2–7 days per spectrum, with baseline counts of up to 30,000 after the Compton correction. Spectra were fit with doublets and sextets using the MEX_FielDD program acquired from the University of Ghent courtesy of E. DeGrave. Values for δ and Δ of the doublets were allowed to vary, and widths (full width at half maximum— Γ , mm/s) of all peaks were coupled to vary in pairs. Errors on isomer shift and quadrupole splitting of well-resolved peaks are usually ± 0.02 mm/s in natural samples [e.g., Skogby *et al.*, 1992], while peak area errors are $\pm 1\text{--}5\%$ depending on the

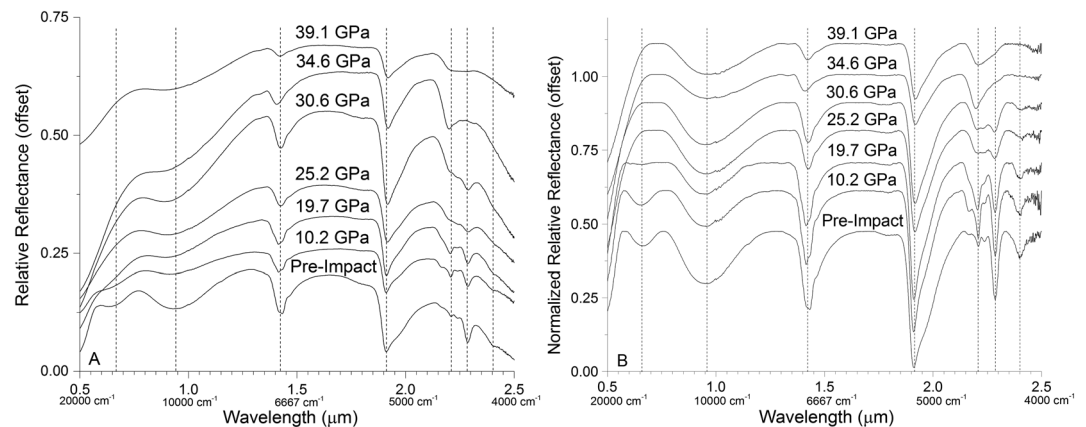


Figure 2. VNIR reflectance spectra of NAU-1 nontronite at controlled RH < 15% after experimental impacts reaching peak pressures between 10.2 and 39.1 GPa. (a) Raw relative reflectance data are compared to (b) normalized relative reflectance data. Data normalization improves the spectral contrast of the metal–OH region between 2.2 and 2.3 μm , which shows increasing disorder in the nontronite octahedral sheet with increasing impact pressure. Normalized data also highlight the retention of the HOH bending overtone of structural H_2O at 1.9 μm after impacts up to 39.1 GPa. Units in wave number (cm^{-1}) have also been provided for secondary reference below the primary X axis units of μm .

degree of peak overlap. For absolute site occupancy measurements based on peak areas (%), saturation corrections and recoil-free fraction effects may be considered, but samples in this study were prepared as thin absorbers and proper values of the recoil-free fraction (f) for these mixed phases were not known, so the areas were not corrected. In this study, the chief interest is in the changes in δ and Δ that occur with shock.

4. Results and Interpretation

4.1. VNIR Reflectance Spectroscopy

Experimental impacts altered the structure of nontronite, producing detectable changes in its VNIR reflectance spectrum (Figure 2). To accurately compare observed changes in nontronite's spectral features with shock, the reflectance spectra of impact-altered nontronite samples were continuum removed and normalized (Figure 2b). This processing ensured that all features were compared from a common basis [Clark, 1999]. Smectites on Mars are primarily identified using VNIR spectroscopy by the presence of characteristic features in the ~ 2.17 – 2.36 μm region, sometimes in association with the 1.4 μm and 1.9 μm hydrated mineral absorptions [e.g., Poulet *et al.*, 2005; Bibring *et al.*, 2006; Mustard *et al.*, 2008]. Because they are so important for phyllosilicate detection and identification, the shifts observed in the 2.2–2.4 μm region of the NAU-1 nontronite VNIR reflectance spectrum after impacts at 39.1 GPa have important implications for the interpretation of remote sensing data from Mars. As these bands derive from characteristic metal–OH overtones and combinations, they are also indicative of changes to the Fe^{3+} bonding environment in the nontronite octahedral sheet. For example, the characteristic $(\text{Fe}^{3+}\text{Fe}^{3+}\text{-OH})$ smectite absorption centered at ~ 2.29 μm shifted to shorter wavelengths, and both the 2.21 μm and 2.165 μm characteristic Al–OH absorption features disappear after impacts at 25.2 GPa and then reemerge as a single, broad feature centered at ~ 2.19 μm after impacts at 34.6 GPa (Figure 3). These spectral changes are consistent with the formation of an aluminum-bearing amorphous phase from the NAU-1 kaolinite contaminant in addition to the breakdown of the nontronite octahedral sheet structure at high peak pressures. At intermediate pressures, however, the VNIR reflectance results for impact-altered nontronite are more difficult to interpret. Differing responses to shock by the components of the octahedral and tetrahedral sheets of nontronite, as well as interaction with the kaolinite contaminant, both contribute to the observed VNIR absorptions in this region.

The sharp Fe–OH vibrational feature centered at 2.29 μm changes from an initial full width at half minimum (similar to full width at half maximum measurements but applicable to reflectance spectra where features are defined by minima instead of peaks) of 0.23 μm to 0.40 μm after shock pressures of 25.2 GPa or higher. A new, single feature centered at 2.2 μm emerges at 34.6 GPa (FWHM = 0.14 μm) and broadens further (FWHM at 39.1 GPa = 0.15 μm) at higher pressures (Figure 3), consistent with the formation of a secondary amorphous

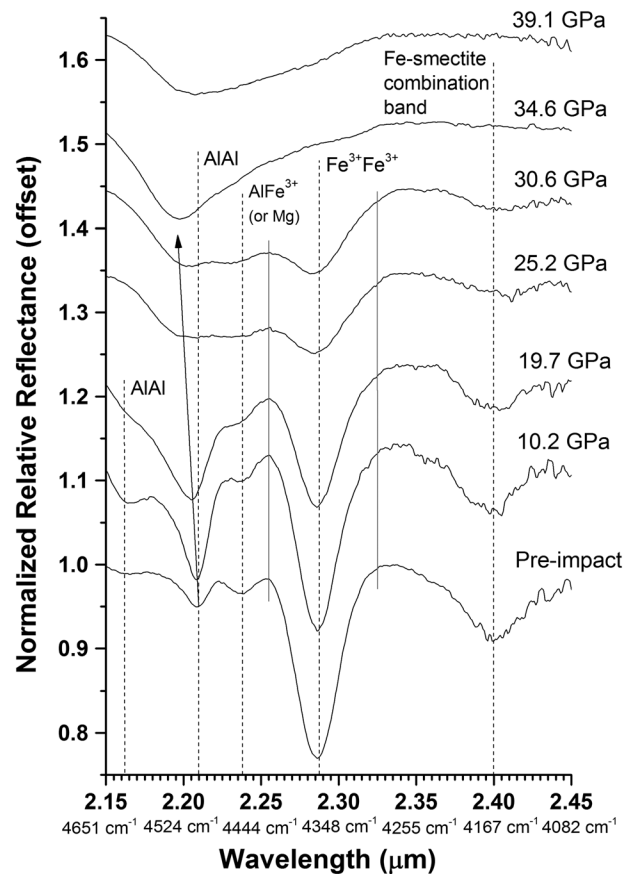


Figure 3. Continuum-removed (ENVI, IDL), normalized (Davinci) comparison of characteristic metal–OH vibrational bands in the M–OH vibrational overtone region of the nontronite VNIR reflectance spectrum. Spectra were taken in controlled relative humidity with $RH < 15\%$. Band identifications are from *Bishop et al.* [2008] and *Bishop et al.* [2002b]. After impacts at or below 30.6 GPa, identifiable metal–OH bands remain; while after impacts 34.6 GPa and above, one broad absorption feature emerges centered at $\sim 2.20 \mu\text{m}$. This broad feature is consistent with VNIR reflectance spectrum of allophane, implying that impact-altered ferruginous smectites may appear as hydrated aluminum-rich amorphous silicates to VNIR reflectance remote sensing techniques. Units of frequency (cm^{-1}) are shown for comparison.

destruction of the Fe^{3+} coordination geometry within the nontronite octahedral sheet [*Che et al.*, 2011; *Che and Glotch*, 2012; *Friedlander et al.*, 2012], or by the production of nanophase iron oxides [*Morris et al.*, 1985] as a result of impact alteration and shock [*Gavin and Chevrier*, 2010; *Gavin et al.*, 2013]. The changes we observed in the metal–OH vibrational features between 2.2 and 2.4 μm , however, support a structural change interpretation favoring distorted Fe coordination geometry without complete OH-group loss (metal–OH vibrational bands are still detected). It is also possible that the impact-altered nontronite sample has been deprotonated, without significant structural change, but if this were the case, then the intensity of the nontronite crystal-field features should increase because O^{2-} is a higher-field ligand than OH^- [*Burns*, 1993], and this is not observed. In addition, no features related to OH-group vibrations would be observed in a completely deprotonated sample.

In addition to mineral-specific identifications, the positions of metal–OH vibrational bands in clay mineral spectra have also been used to identify characteristic cations [*Bishop et al.*, 2002b]. Variations in the shapes and locations of these bands have been attributed to varying Fe/Mg abundances [*Poulet et al.*, 2005]. It is

phase. A weaker Al–OH vibrational feature (associated with the NAU-1 kaolinite contaminant) centered at 2.2 μm is retained up to 19.7 GPa and disappears completely between 19.7 and 25.2 GPa, to be replaced by the single 2.2 μm feature at peak pressures of 34.6 GPa and above (Figure 3). These results are consistent not only with structural deformation in the octahedral sheet that begins at low pressures but also with a structure that is not completely deformed until relatively high peak pressures are achieved. The retention of hydroxyl groups by impact-altered nontronite means that the structurally deformed sample still produces a (spectrally different) VNIR reflectance spectrum with metal–OH overtones in the characteristic phyllosilicate region (2.17–2.36 μm). The fact that impact-altered nontronite produces a spectroscopically distinct spectrum and is structurally deformed rather than completely dehydroxylated has important implications for Martian remote sensing.

Band center and intensity shifts in the extended visible wavelength region of the impact-altered nontronite VNIR reflectance spectrum provided further evidence for structural change in the nontronite octahedral sheet after impacts. Nontronite has two characteristic Fe^{3+} crystal-field absorptions at 0.65 and 0.87 μm that are attributed to octahedrally coordinated Fe^{3+} cations [*Burns*, 1993]. At shock pressures of 19.7 GPa and above, a broad, asymmetric feature centered at $\sim 1.0 \mu\text{m}$ replaces nontronite's two Fe^{3+} crystal-field absorptions (Figure 2). This may be explained by partial dehydroxylation or

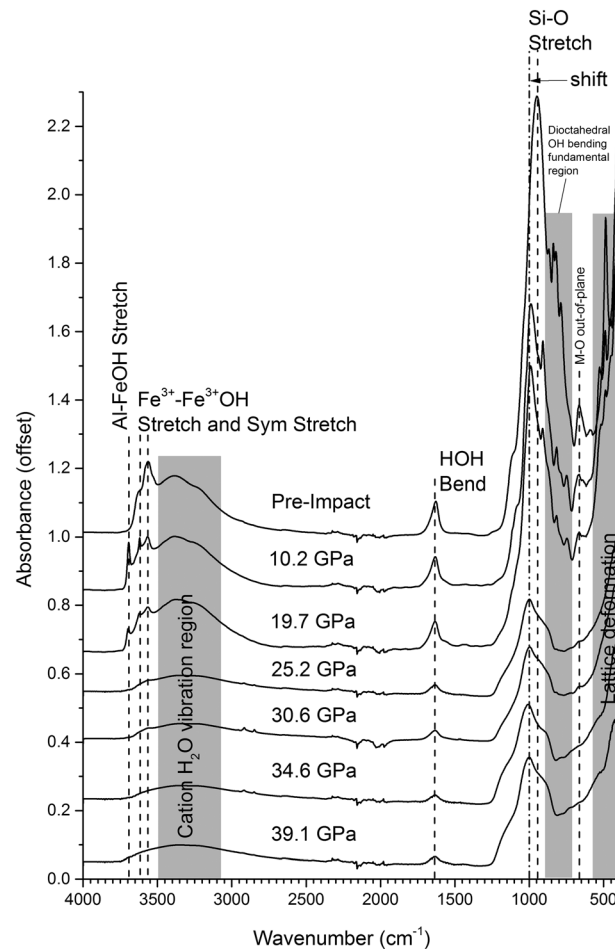


Figure 4. MIR ATR spectra of NAU-1 nontronite after experimental impacts reaching peak pressures between 10.2 and 39.1 GPa. Shifts in the Si–O stretching and M–MOH bands are consistent with extensive octahedral sheet deformation. Wavelength units in μm are shown for comparison with the standard X axis units of frequency (cm^{-1}). Band assignments are based on Frost and Klopogge [2000], Bishop et al. [2002a, 2002b], and Neumann et al. [2011]. The Al–FeOH stretch band ($\sim 3700 \text{ cm}^{-1}$) has also been identified as a kaolin contaminant [Keeling et al., 2000].

associated with O–H stretches from structural H_2O or metal–OH stretching [Clark et al., 1990]. Lower frequency features arise from Si–O stretching (1000 cm^{-1}), metal–metal–OH deformations ($908\text{--}742 \text{ cm}^{-1}$), Si–O–metal bends ($\sim 500 \text{ cm}^{-1}$), and long-range silicate lattice deformations ($\sim 600\text{--}400 \text{ cm}^{-1}$) [Clark et al., 1990; Bishop et al., 2008].

The nontronite ATR spectrum changed dramatically above 19.7 GPa shock pressure (Figure 4). The broad (structural H_2O) O–H stretching band at 3400 cm^{-1} substantially weakened at pressures above 19.7 GPa, which is consistent with the trend observed for both the 1.4 and 1.9 μm hydration absorption features in the VNIR reflectance spectrum of nontronite. In contrast, the 1630 cm^{-1} H_2O H–O–H bending absorption feature was retained up to 39.1 GPa, although this was probably due to the presence of adsorbed H_2O on the surfaces of the analyzed phyllosilicate grains. The intensity of the sharp Si–O–Fe bending feature (484 cm^{-1}) decreased by nearly 80% after exposure to experimental impacts with the relatively low peak pressure of 19.7 GPa (Figures 4 and 6), reflecting the combined effects of structural deformation in both the octahedral and tetrahedral sheets of the nontronite structure. The Al–Fe–OH (908 cm^{-1}), Fe–Fe–OH (808 cm^{-1}), and Mg–Fe–OH (742 cm^{-1}) deformation features (second shaded region in Figure 4, labeled “diocahedral OH

possible, however, that variability in band shape and location might also be due to impact shock. The changes to the nontronite $2.29 \mu\text{m}$ Fe–OH vibrational feature that we describe above are similar to the shifts in band depth and center attributed by Poulet et al. [2005] to changes in the Fe/Mg abundance ratios of the phyllosilicate deposits that they identified on Mars. Therefore, we propose impact shock as a possible alternative explanation for variations in the depths and locations of the 2.2–2.4 μm region bands in Martian phyllosilicate spectra. In addition, the presence of Al in our natural nontronite sample has a strong effect on the band center of the broad metal–OH band that emerges after impacts at 39.1 GPa (Figure 3). Because we used the same nontronite sample throughout, we know that the impact-altered, high-pressure samples are still iron rich (and this is confirmed by our Mössbauer spectroscopy results), but an amorphous, Al-rich phase dominates these VNIR reflectance spectra. This has implications for the identification of Al-rich phyllosilicates in heavily bombarded regions of Mars [Rampe et al., 2012; Bishop and Rampe, 2014], because it is possible that structurally deformed iron-rich phases may be present but not detected in these regions.

4.2. MIR ATR Spectroscopy

MIR ATR spectroscopy probes both the hydroxyl and silicate parts of the phyllosilicate structure. High-frequency features between 3000 and 3700 cm^{-1} are

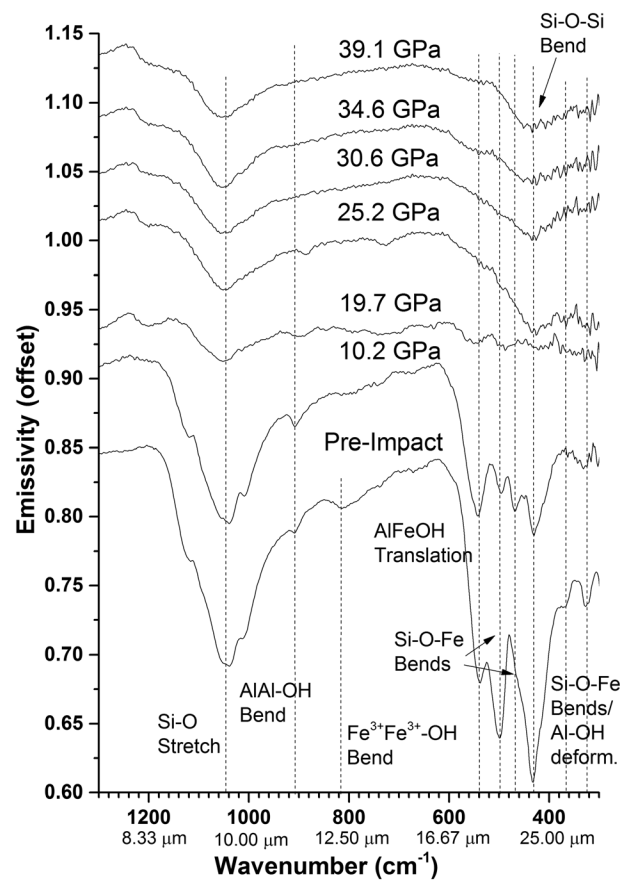


Figure 5. MIR emissivity spectra of NAu-1 nontronite after experimental impacts reaching peak pressures between 10.2 and 39.1 GPa. Loss of the characteristic lattice deformation bands of nontronite ($600\text{--}400\text{ cm}^{-1}$) and the weak OH bending fundamental bands ($950\text{--}725\text{ cm}^{-1}$) supports a hypothesis of increasing octahedral sheet disorder with increasing impact pressure. After impacts of 19.7 GPa and higher, the emissivity spectrum of nontronite is indistinguishable from amorphous, hydrated silica. Band assignments were based on Frost and Klopogge [2000] and Neumann *et al.* [2011]. Wavelength values (μm) corresponding to standard frequency units (cm^{-1}) have been included for comparison.

the amorphous Al-rich secondary phase begins to form at peak pressures of ~ 35 GPa. The Al-Fe-OH deformation feature at 908 cm^{-1} also persists to 19.7 GPa and above (as a weak shoulder on the 1000 cm^{-1} Si-O stretch). The retention of Al-OH features suggests that Al phyllosilicates may be more structurally resilient after impacts than Fe-rich clays. This result is consistent with previous research on the thermal alteration of clays [e.g., Gavin and Chevrier, 2010; Che *et al.*, 2011]. Reported empirical thermodynamic data also show that the Al-OH bond is stronger than the Fe-OH bond [e.g., Haynes and Lide, 2010]. Similar effects have also been observed after weathering clay minerals in acidic conditions [Altheide *et al.*, 2010; Craig *et al.*, 2014].

4.3. MIR Emission Spectroscopy

MIR emission spectroscopy is primarily sensitive to structural deformation in the tetrahedral sheet of nontronite. Because it is dominated by silicate bends and stretches, MIR emission spectroscopy provides the most information about changes to the Si bonding environment within the interconnected rings of SiO_4 silicate tetrahedra that make up the nontronite tetrahedral sheet. Initial deformation begins at higher pressures in the tetrahedral sheet than in the octahedral sheet. For example, the MIR emissivity spectrum of nontronite after an impact at 10.2 GPa peak pressure still contains many diagnostic features and is largely

bending fundamental region") were reduced to a single broad shoulder after impacts at 25.2 GPa or higher. Because all of these spectral changes occurred over a range of peak pressures, we hypothesize that impact shock structurally deformed different parts of the nontronite structure at different rates. However, both the tetrahedral and octahedral sheets are severely deformed by impacts at pressures of 30.6 GPa and higher. Thus, we also hypothesize that structural degradation after impacts does not proceed in a completely progressive, stepwise manner (like thermal alteration), but rather that characteristic components of the structure may be maintained until a high-pressure "tipping point" (>19.7 GPa) is reached, beyond which nontronite becomes spectrally amorphous, though not completely devolatilized.

The ATR spectra of postshock nontronite also demonstrate spectral differences between iron in the nontronite structure with that on aluminum in kaolinite. Although the strength of the Fe-OH stretching band at 3550 cm^{-1} progressively declines from a 10.0 GPa shock onward, an Al-FeOH stretching band at 3620 cm^{-1} emerges with increasing contrast from the shoulder of the broad nontronite 3400 cm^{-1} hydration band. Unlike their Fe-OH counterparts, the band depths of Al-OH features do not decrease until after impacts at pressures of 19.7 GPa and above, and they reemerge as

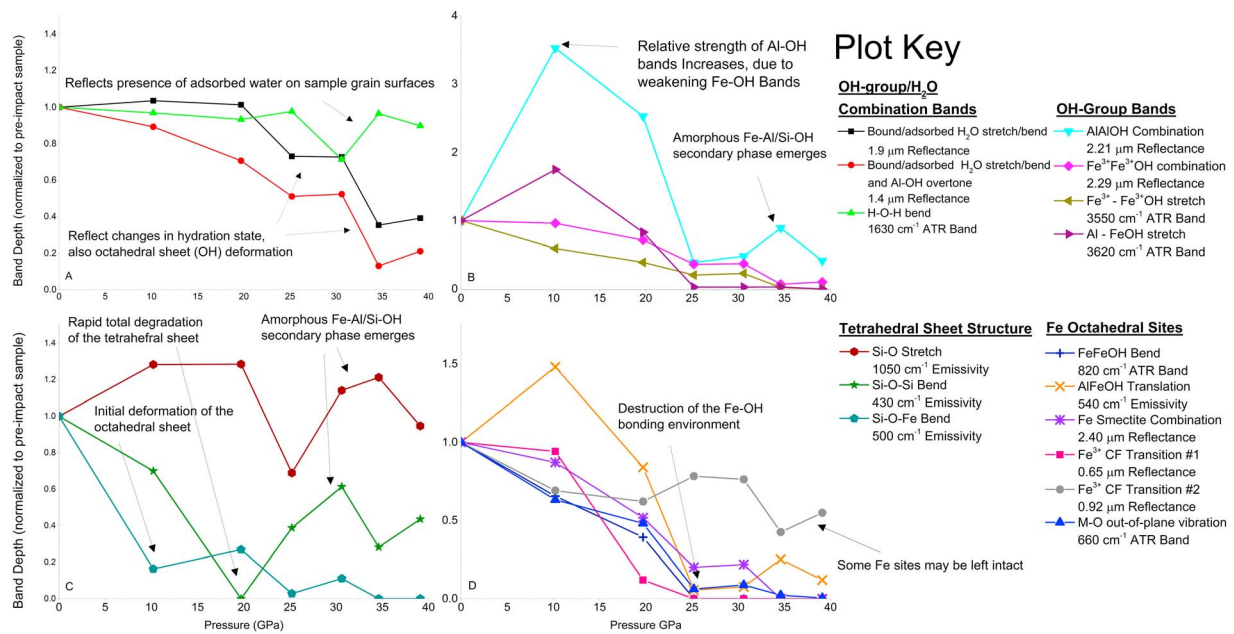


Figure 6. Changes in the depths [after *Pelkey et al., 2007*] of various characteristic nontronite bands with increasing pressure, reflecting alteration to various parts of the nontronite structure. (a) Bands related to structural H₂O, adsorbed H₂O, and hydroxyl overtone and combination vibrations, (b) bands related to OH-group vibrations characteristic of nearby cations, (c) tetrahedral Si-site vibrations, and (d) bands reflective of the Fe-octahedral environment, although these are also reflected in the changes to the OH-group bands. Because different parts of the structure experience different degrees of alteration with increasing pressure, these band depth changes demonstrate how it is possible to observe seemingly contradictory spectral results from techniques that probe different parts (and length scales) of the nontronite structure. ATR spectra were converted to reflectance before band depths were analyzed by relating reflectance to absorbance ($R = 1/10^{Abs}$). All spectra were continuum removed using ENVI/IDL and were normalized in Davinci (excepting the M-O out-of-plane band, which was too noisy to normalize) prior to comparison and analysis.

unchanged from the unaltered spectrum (Figure 5). However, total structural degradation proceeds more quickly and occurs at lower pressures in the tetrahedral than in the octahedral sheet. After only a 19.7 GPa shock, the emission spectrum of nontronite changed substantially, and diagnostic spectral features could no longer be detected. These results imply that structural deformation in the octahedral sheet proceeds gradually, increasing almost linearly with pressure, while deformation in the tetrahedral sheet proceeds suddenly, passing rapidly into spectrally amorphous material after impacts at intermediate pressures. In contrast to other Si-O vibrational bands, the Si-O stretching band around 1000 cm⁻¹ became progressively broader with increasing shock pressure but could always be detected. This implies that Si-O bonds are retained even as the long-range ordered structure of the silicate tetrahedra begins to break down. This is largely consistent with the changes to the nontronite octahedral-layer observed using ATR and VNIR reflectance spectroscopy, and described in the preceding sections. There is some evidence from solid state chemistry that MIR spectroscopic techniques are particularly sensitive to structural disorder [*Tarte et al., 1990*], implying that these results may be due to the sensitivities of the techniques used rather than different responses to shock by different parts of the nontronite structure. However, MIR spectroscopic techniques are uniquely sensitive to changes in the bonding environment of a clay mineral's tetrahedral sheet, and the observed spectral changes differ for different parts of the nontronite structure. The complete deformation of the tetrahedral sheet that occurs at a lower pressure than that observed for the octahedral sheet (Figure 6) produces spectra at intermediate peak pressures that resemble amorphous silicates in the MIR (Figures 4 and 5), while retaining characteristic Fe-OH nontronite bands in the VNIR (Figures 2-4).

4.4. Band Depth Change Comparisons Between Multiple Spectroscopic Techniques

Impacts induced structural deformations in different parts of the nontronite structure at different peak pressures, producing measurable differences in the changes to band depths and band center for characteristic spectroscopic features, as measured by multiple spectroscopic techniques (Figure 6). In particular, deformation of the octahedral sheet begins at a lower pressure but is not complete until a higher pressure than deformation of the tetrahedral sheet (Figures 6b-6d). The effect of adsorbed H₂O on our

results is clear (Figure 6a), but the changes observed in the 1.4 and 1.9 μm absorption features also trend with octahedral sheet and metal–OH interaction deformations (Figures 6b and 6d). Therefore, it is likely that both hydration state changes and changes to the OH-group bonding environment as a result of impacts may have contributed to the shifts observed for these bands. This has important implications for detecting the smectite-to-illite transition and diagenesis by remote sensing using the 1.4 and 1.9 μm hydration bands as proxies for relative hydration state [e.g., Milliken, 2014]. Such results should be interpreted with caution due both to the complexities of the bands themselves and to the possibility of combined processes, which may produce similar spectroscopic results.

Changes in band depth may also result from increasing grain size [Clark, 1999]. This is especially important to note for our nontronite sample because we observed that the finely ground original sample powder was occasionally physically pressed into large flakes by the experimental impacts, especially at high peak pressures. However, comparisons between VNIR reflectance spectra taken separately of these postimpact flakes and spectra of the bulk sample indicated that there were no significant spectral differences between the two. This indicates that the observed differences between the preimpact and postimpact VNIR reflectance spectra of our nontronite sample arise from impact-induced structural changes and not pressure-related physical changes to the sample. These results further indicate that postimpact nontronite may still be identified as either a semi-amorphous phyllosilicate, hydrated amorphous silicate, or a smectite of indeterminate species by VNIR reflectance spectroscopy using the presence of the broad ~ 2.2 μm band (in combination with 1.4 and 1.9 μm hydration features), even after experimental impacts up to 39.1 GPa. Most importantly, however, at intermediate impact pressures, differing effects of shock on the tetrahedral and octahedral sheets of the nontronite structure produced seemingly contradictory spectral results. In particular, MIR spectra resembled nonspecific hydrated amorphous silicates after the tetrahedral sheet deformed, but characteristic nontronite vibrational bands from the more resilient octahedral sheet were still detected by VNIR reflectance spectroscopy.

4.5. Raman Spectroscopy

With iron-rich minerals (such as nontronite), the sensitivity of Raman spectroscopy to small changes in the bonding environments of samples often results in high fluorescence and low signal/noise. We attempted to mitigate these effects by using a 785 nm laser, but we still found that useful Raman spectra were extremely difficult to collect from samples exposed to impacts above 10 GPa. These results confirm the observations of Gavin *et al.* [2013], who found that many of their samples produced nearly “featureless” Raman spectra. They attributed these results to “...irregular fracturing, imperfections, amorphous phases, and/or water in the samples.” Gavin *et al.* [2013] did not conclude that the changes observed in their Raman spectra were produced by impact shock, but they suggest that this may be the case. Based on our preimpact Raman spectra and postimpact featureless spectra (Figure 7), we find that Raman spectroscopy is extremely sensitive to shock-induced structural change, that postimpact clay minerals do not produce interpretable Raman spectra, and that this is likely a direct result of their exposure to experimental impacts.

4.6. Transmission Electron Microscopy

TEM images of both shocked and unshocked nontronite samples were acquired (Figure 8). The dispersed particles of unshocked nontronite are polycrystalline aggregates with complex morphologies and significant structural disorder. These particles are aggregates of (001) flake-like crystallites (Figures 8a, 8d, and 8g) with curled edges that expose packets of clay layers suitable for high-resolution transmission electron microscopy (HRTEM) imaging of the (001) lattice fringes (Figures 8c, 8f, and 8i). Selected area electron diffraction (SAED) patterns of the aggregate particles consist of nearly continuous rings corresponding to reflections in the [001] zone axis (Figures 8b, 8e, and 8h), which indicates that the particles are aggregates of oriented (001) flakes. The continuous rings in the [001] patterns indicate turbostratic disorder (rotation about the [001] stacking direction) within and among the clay crystallites that make up the aggregate. HRTEM imaging of some nontronite crystallites shows packets of (001) lattice fringes indicating clay crystals up to about 60 nm thick (Figure 8c). The complex and disordered structure of these unshocked particles makes documentation of shock-induced deformation difficult.

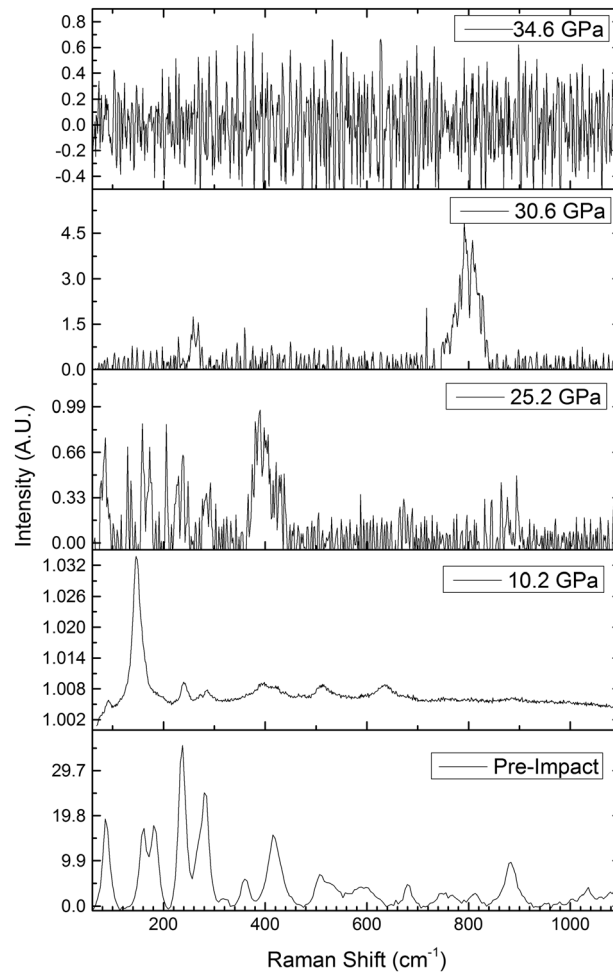


Figure 7. Raman spectra of NAu-1 nontronite after experimental impacts between 10.2 and 39.1 GPa, background removal, and processing performed in WITec Project Plus software. No signal could be detected for the sample exposed to an experimental impact of peak pressure 19.7 GPa, so it is not included. The preimpact spectrum was taken using the 532 nm laser setup, while all postimpact spectra were taken using the 785 nm laser setup to try and reduce fluorescence. Nonetheless, fluorescence increases with increasing pressure, while signal decreases correspondingly.

~4.4 Å ring is barely visible, indicating some local crystallinity. Many HRTEM images are consistent with a complete loss of long-range order, but some crystallites with visible (001) lattice fringes are present (Figure 8i). As observed in other samples, the shock effects are heterogeneous and the local regions of nanocrystallinity may not be representative of the bulk 39.1 GPa sample. These results are consistent with the progressive onset of structural deformation occurring in different parts of the nontronite structure at different rates.

4.7. X-Ray Diffraction

XRD data for the preimpact nontronite sample (Figure 1) show features typical of nontronite, with a 001 peak at ~15.2 Å (~6° 2θ) and a variety of *hkl* bands reflecting turbostratic stacking (e.g., the 02*l*, 11*l* band beginning at ~19.5° 2θ, and the 06*l*, 33*l* band at ~60.8° 2θ). The 15.2 Å basal spacing (001) is consistent with two layers of H₂O molecules in the interlayer region (data measured at 44% relative humidity). The data also reveal the presence of kaolinite, whose 001 and 002 reflections are indicated. XRD data for the

The onset of shock deformation is visible in samples shocked to 19.7 and 24.6 GPa, but the shock-induced changes are subtle. Morphologically, the particles of nontronite shocked to 19.7 and 24.6 GPa are nearly the same as the unshocked material, but the crystallites are generally smaller and more disordered (Figures 8d–8i). SAED patterns, like those of the unshocked nontronite, show turbostratic disorder in their (001) zone-axis patterns. The SAED patterns have the same inner rings as the unshocked material (4.4 Å and 2.5 Å), but the diffraction intensity is weaker, and the higher-order rings are absent (Figures 8e and 8h). This loss of diffraction intensity indicates loss of structural order. HRTEM images showing (001) lattice fringes indicate that the crystallites are smaller and more deformed than those observed in the unshocked material. Samples shocked to 30.6 and 35.6 GPa have similar morphologies, but the crystallite size and the diffracted intensities of higher-order rings are further reduced. Some patterns have only one diffuse ring, indicating nearly complete amorphization. HRTEM imaging shows curved crystallites up to 20–30 nm thick, but they are fewer than in lower pressure samples.

Nontronite shocked to 39.1 GPa is morphologically similar to samples from 35.6 GPa, but SAED indicates that the samples shocked to 39.1 GPa are predominantly amorphous (Figures 8g–8i). SAED patterns generally show no distinct diffraction rings, indicating that the material is almost completely amorphous. Figure 8h shows an example where the

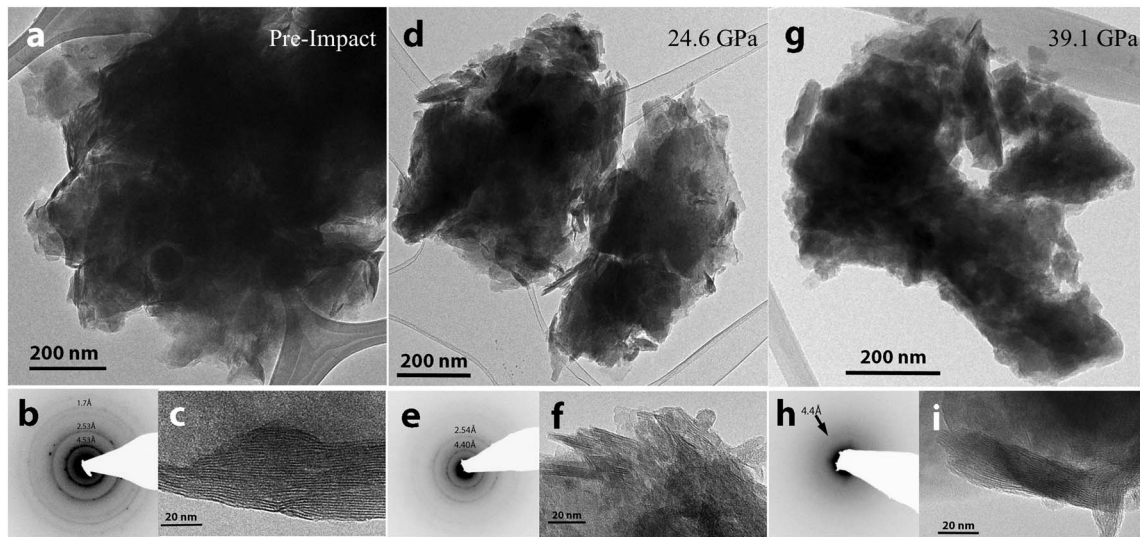


Figure 8. Bright field images of aggregate particles of (a) unshocked as well as shocked nontronite after impacts up to (d) 24.6 GPa and (g) 39.1 GPa with (b, e, h) associated selected area electron diffraction (SAED) patterns and (c, f, i) HRTEM images of specific crystallites. Both the unshocked and 24.6 GPa samples consist primarily of flat (001) crystallites with curled edges, which appear as fibrous structures around the edges of the flakes in the bright field images (Figures 8a and 8d). The unshocked SAED pattern (Figure 8b) shows rings from reflections in the [001] zone axis with no reflections or rings corresponding to 001 reflections. The continuous rings indicate turbostratic disorder in and between the nontronite crystallites. The ring d-spacings 4.53, 2.53, and 1.7 Å are illustrated for the unshocked sample (Figure 8b) for comparison to other SAED patterns (Figures 8e and 8h). The HRTEM image of unshocked nontronite (Figure 8c) shows a 60 nm thick packet of clay (001) layers. The SAED pattern of nontronite shocked up to 24.6 GPa shows the same [001] turbostratic ring structure as that produced by unshocked nontronite, but the higher-order ring intensity is somewhat reduced. The HRTEM image (Figure 8f) shows (001) lattice fringes in smaller and more disrupted crystallites. The SAED pattern of nontronite shocked up to 39.1 GPa, on the other hand, has only a trace of the 4.4 Å ring indicating that this aggregate is nearly amorphous. However, the HRTEM image of a different particle from this sample (Figure 8i) shows clear (001) lattice fringes, indicating that some order survives in the clay structure.

postimpact samples are compared with those for the preimpact material in Figure 9. These data reveal no significant modifications to the structure after impacts up to 10.0 and 19.7 GPa, as reflected by the persistence of the basal and *hkl* features. Data for the samples shocked at 25.2 GPa and above show a gradual intensity decrease and broadening of the 001 reflection, loss of detail for *hkl* features, and gradual increase in a broad scattering feature from ~ 15 to $40^\circ 2\theta$. Such a broad feature is generally indicative of the presence of an amorphous phase [Ohashi *et al.*, 2002; Music *et al.*, 2011; Rouff *et al.*, 2012], and this scattering feature probably reflects the increasing, progressive amorphization of the nontronite and kaolinite with increasing peak shock pressure. The minor feature near $44.6^\circ 2\theta$ is from the sample substrate. All samples were analyzed at approximately the same relative humidity ($44 \pm 4\%$). The intensity of the 001 reflection gradually decreased as a function of pressure, and Figure 9 also illustrates that the width of the 001 reflection increased significantly from 19.7 to 34.6 GPa. The value of $d(001)$ also decreased slightly as a function of pressure, from ~ 15.3 Å in the untreated material to ~ 14.4 Å at 25.2 GPa and 13.9 Å at 34.6 GPa, showing that all materials other than the 39.1 GPa sample retained the ability to incorporate interlayer H₂O molecules. Due to the small amounts of available sample, the y axes for some patterns (Figure 9) were expanded by a factor of 4 to increase the contrast in these figures and demonstrate that characteristic peaks are still present.

4.8. Mössbauer Spectroscopy

Earlier Mössbauer studies of other ferruginous smectites, including nontronite [Bishop *et al.*, 1999] fit nontronite spectra with four Fe³⁺ doublets, namely two octahedral ($\sim 90\%$ of the total Fe) and two tetrahedral ($\sim 10\%$). The presence of tetrahedral Fe³⁺ was also supported by the existence of a band near $22,000$ cm⁻¹ (0.45 μm) in their optical spectra. However, subsequent chemical analyses [Bishop *et al.*, 2002b, 2002c, 2008; Dyar *et al.*, 2008] showed sufficient Si and Al ions to fill all tetrahedral sites, and Bishop *et al.* [1999] noted some heterogeneity in their nontronite sample. In light of this equivocal evidence for the site occupancy of Fe in nontronite, several different methods were initially used to fit the Mössbauer spectra in this study, using the same methods employed in Dyar *et al.* [2008]. As in the 2008 study, attempts to model both octahedral and tetrahedral Fe³⁺ doublets resulted in large values of χ^2 and random changes in doublet areas, δ and Δ .

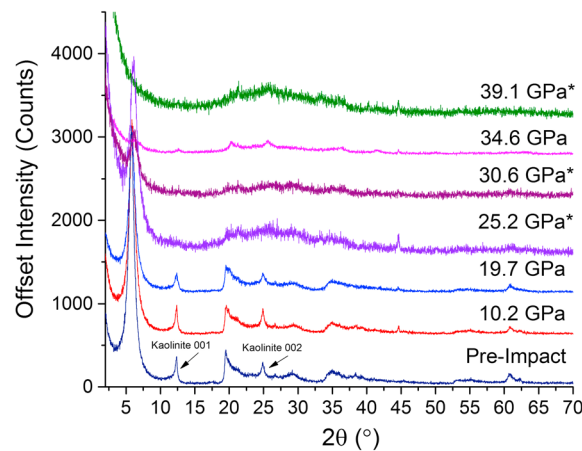


Figure 9. X-ray diffraction patterns of NAU-1 nontronite exposed to experimental impacts with peak pressures between 10.2 GPa and 39.1 GPa. Structural disorder, indicated by decreasing peak intensities and peak broadening as well as the emergence of a broad “amorphous” feature ($20^\circ < 2\theta < 40^\circ$), generally increases with increasing peak impact pressure but was not observed with XRD below pressures of 25.2 GPa. Small amounts of analyzable sample led to increased noise in some diffraction patterns, especially at impact pressures above 19.7 GPa. *Intensity expanded by 4.

fully oxidized at all shock pressures, but the Fe^{3+} parameters suggest that the octahedral site is increasingly distorted.

5. Discussion

5.1. Observations From the Use of a Natural Nontronite Sample: Contaminant Effects

The nontronite standard NAU-1 is known to contain kaolinite [Keeling *et al.*, 2000]. Contaminant effects are a major drawback of using natural mineral samples in laboratory spectroscopy. Through careful band assignments, however, we can identify the spectroscopic features associated with kaolinite and use them to compare the effects of shock on kaolinite with those observed for nontronite. In general, we found that kaolinite bands were detected more strongly after higher-pressure impacts than nontronite bands were. We interpret this to mean that the kaolinite structure may be better able to withstand the disordering effects of

Two-doublet models with only octahedral Fe^{3+} doublets produced the lowest values of χ^2 and the most systematic changes in δ with temperature.

Results of the current study therefore reproduce the results of Dyar *et al.* [2008] in the unshocked material (Table 2). A majority (88%) of the Fe^{3+} in this sample is in the doublet with parameters of $\delta = 0.37$ mm/s and $\Delta = 0.34$ mm/s. A smaller doublet initially has 12% of the total area, with parameters of $\delta = 0.37$ and $\Delta = 0.69$ mm/s. Because Δ generally increases with site distortion [Dyar *et al.*, 2006], this latter doublet is interpreted to be a more distorted local environment in the nontronite six-coordinated sites. As the intensity of the shock increases to 19.7 GPa, Fe^{3+} partitions away from the low- Δ doublet and into the higher- Δ doublet (Figure 10). At 25.2 GPa and above, there is no occupancy of an undistorted site with low Δ ; instead, a third type of site that is even more distorted occurs with $\delta = 0.35$ – 0.36 mm/s and $\Delta = 1.14$ – 1.19 mm/s. These results show that Fe^{3+} in nontronite remains

Table 2. Parameters for the 295k Mössbauer Spectra of All Samples Analyzed in These Experiments^a

Fe ³⁺ Doublet	Mössbauer Parameter	Nontronite Sample						
		Preimpact (NAU-1)	10.2 GPa	19.7 GPa	25.2 GPa	30.6 GPa	34.6 GPa	39.1 GPa
Doublet 1	δ (mm/s)	0.37	0.37	0.36	--	--	--	--
	Δ (mm/s)	0.34	0.34	0.34	--	--	--	--
	Γ (mm/s)	0.46	0.44	0.44	--	--	--	--
	Area (%)	88	85	57	--	--	--	--
Doublet 2	δ	0.37	0.36	0.35	0.33	0.36	0.34	0.35
	Δ	0.69	0.75	0.75	0.67	0.50	0.63	0.71
	Γ	0.23 ^b	0.35	0.43	0.48	0.40	0.38	0.34
	Area	12	15	43	68	55	28	42
Doublet 3	δ	--	--	--	0.36	0.35	0.35	0.35
	Δ	--	--	--	1.14	1.21	1.16	1.23
	Γ	--	--	--	0.36	0.38	0.49	0.46
	Area	--	--	--	32	45	72	58

^aNot every sample fits iron with every doublet; parameters for doublets that were not needed to fit a given sample’s spectrum have been left blank.

^bFixed parameter.

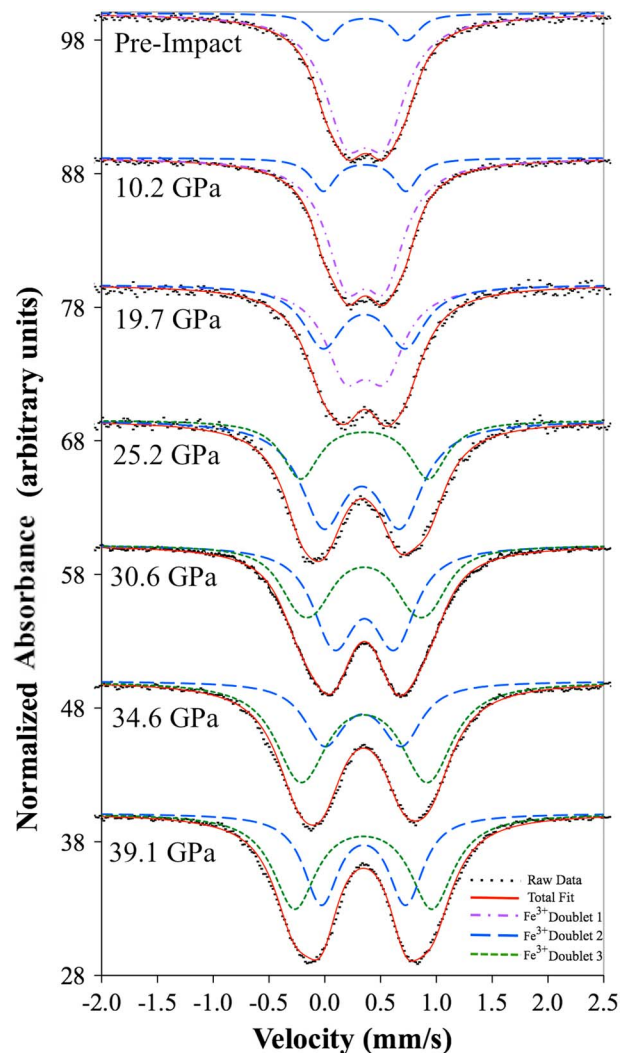


Figure 10. Mössbauer spectra of NAu-1 nontronite exposed to experimental impacts between 10.2 and 39.1 GPa. The results indicate that although all iron begins (and remains) in the oxidized, ferric state (Fe^{3+}), the iron coordination geometry in the octahedral sheet becomes increasingly disordered as peak impact pressure increases.

5.2. Comparison of Shock and Thermal Alteration

The effects of thermal alteration on clay mineral structure and spectroscopy have been extensively addressed by previous laboratory spectroscopy work [Boslough *et al.*, 1986; Gavin and Chevrier, 2010; Che *et al.*, 2011; Daly *et al.*, 2011; Che and Glotch, 2012]. These results showed that thermal alteration proceeds via the dehydration and dehydroxylation of clay mineral structures, eventually leading to layer collapse and the formation of amorphous phases, followed by the recrystallization of secondary phases, such as cristobalite, hematite, and anorthite [Gavin and Chevrier, 2010; Che *et al.*, 2011]. In contrast, our results suggest that shock produces different structural and spectroscopic changes in nontronite than those produced by thermal alteration. This conclusion supports the early findings of Boslough *et al.* [1986], who first observed that color change in shocked nontronite samples differed from that induced by annealing (thermal alteration). It also suggests that the color changes observed in shocked nontronite by Weldon *et al.* [1982] were likely a result of both shock-induced stress and thermal alteration rather than shock-induced thermal alteration alone. It is important to understand the effects of shock and temperature as separate processes because (with the exception of very large impacts) the nonlinear relationship between pressure and temperature in impacts

impacts, and that kaolinite is less susceptible to spectral change after experimental impacts, which is consistent with the relative strengths of Fe–OH (weaker) versus Al–OH (stronger) bonds [Haynes and Lide, 2010]. This is in contrast to the results reported in Gavin *et al.* [2013], who found that their nontronite sample partially retained its structure, whereas the structure of their postimpact kaolinite sample was shown by XRD to be completely destroyed. The difference between our results may be explained by the fact that the nontronite sample in Gavin *et al.* [2013] was exposed to an impactor velocity of 3.27 km/s, which they modeled as corresponding to a peak pressure of 17.5 GPa, whereas the kaolinite sample was exposed to a higher impactor velocity of 4.3 km/s, although velocity and stress (i.e., pressure) cannot be directly compared [Kraus *et al.*, 2013]. We also hypothesize that the presence of Al in our nontronite sample may be partially responsible for the broad singlet feature centered at $\sim 2.2 \mu\text{m}$ that emerges in the VNIR reflectance spectra of NAu-1 exposed to impacts at 34.6 GPa or higher (Figure 5). The fact that Al-based bands dominate the spectrum of an Fe-rich material after impact at high pressures has important implications for the interpretation of planetary remote sensing data. In the case of our sample, the altered high-pressure spectrum of nontronite, which is dominated by an amorphous Al-bearing, hydrated silicate, would imply that it is Fe poor, when it is in fact impact-altered, Fe-rich nontronite in the presence of a potentially Al-rich, amorphous secondary phase.

makes it unlikely that shocked material would experience temperatures significantly higher than 500°C for extended time periods [French, 1998]. One important exception to this is localized heating in sample pore spaces. As Gavin *et al.* [2013] showed, it is possible to reach extremely high but very spatially localized temperatures in samples exposed to impact shock. For this reason, they concluded that their results showed the combined effects of temperature and pressure. However, we used the technique of shock reverberation to achieve peak pressure, which produces less entropy [Kraus *et al.*, 2013] and results in lower peak heating [Gibbons and Ahrens, 1971]. Although we did not measure the peak temperatures achieved during our impact experiments, previous work has shown that shock-reverberation sample holders only reach temperatures in the range of 130–200°C [Raikes and Ahrens, 1979; Boslough *et al.*, 1980], which are not hot enough to devolatilize bound OH from nontronite [Frost *et al.*, 2002]. Thus, we suggest that the structural (and spectral) changes to our samples were generated primarily by shock and not high temperatures. Further work is warranted to explore the different effects of these two processes on phyllosilicate structure and spectroscopy. However, the distinct spectral changes we report, and the differences between them and those reported for thermally altered nontronite, demonstrate that shocked and thermally altered phyllosilicates are spectroscopically distinct up to pressures of ~40 GPa and both should be accounted for in future analyses of planetary remote sensing data.

5.3. Implications for the Remote and In Situ Sensing of Mars

Our results indicate that structural deformation after impact shock may be detected at slightly different peak pressures by spectroscopic techniques sensitive to change in different parts of the nontronite structure. The onset of deformation in the octahedral sheet occurs at the relatively low peak pressure of 10.2 GPa, indicated by band depth changes related to structural change in nontronite's octahedral sites (Figure 6), but total deformation and related spectral changes are not observed until higher pressures. Characteristic Fe–OH bands are detectable at pressures up to 25.2 GPa. In contrast, characteristic spectral features arising from the vibrations of the Si–O bands in the tetrahedral sheet are initially unaffected, but after impacts at peak pressures of only 19.7 GPa, the intensity of the Si–O–Fe bending feature (500 cm^{-1}) decreased by >70%, while the Si–O–Si bending feature (430 cm^{-1}) was undetectable (Figure 6). At these same pressures, characteristic Fe–OH features from the octahedral sheet of nontronite can still be detected in the VNIR wavelength range (Figures 6b and 6d). As a result, impacts of intermediate peak pressures can produce spectrally amorphous MIR detections, which may correspond with characteristic nontronite detections using VNIR reflectance spectroscopic techniques. In addition, impact alteration eventually produces an amorphous secondary phase, an Al-bearing (possibly also Fe bearing, though this is unclear) amorphous hydroxylated silicate. This secondary phase dominates the spectrum of impact-altered nontronite after experimental impacts at high pressures.

There are two important implications for the remote sensing of the Martian surface that can be derived from these observations. First, shocked phyllosilicate spectra should be included in the spectral libraries used to identify minerals from planetary remote sensing data. Shocked nontronite is spectrally distinct from unshocked nontronite and should be included as a distinct end-member. It is therefore important to acquire a complete library of laboratory-shocked phyllosilicate spectra. Second, impact alteration and related processes may explain the challenges experienced by researchers attempting to identify phyllosilicates from TES and THEMIS MIR spectral data. Impact-induced structural disorder, which deforms the octahedral and tetrahedral sheets of nontronite differently, produces different spectral effects in the MIR and the VNIR wavelength detection regions. Because MIR remote sensing techniques are primarily sensitive to the Si–O fundamental bending and stretching vibrations of the tetrahedral sheet, while VNIR reflectance techniques are sensitive to characteristic metal–OH combination and overtone bands, structural deformation in the tetrahedral sheet but not the octahedral sheet may lead to spectrally amorphous MIR detections but unambiguous VNIR detections.

Our results also have important implications for the specific identification of clay minerals by characteristic cation–OH absorptions [e.g., Poulet *et al.*, 2005; Bishop *et al.*, 2008]. Our results show that impact-induced structural disorder causes the spectrum of Fe-rich NAu-1 nontronite to become dominated by a secondary Al-bearing amorphous silicate phase. The effects of shock on the sample's kaolinite contaminant produce this phase, demonstrating the complexity of interpreting spectral results from shocked mineral mixtures (and natural samples). This effect may be especially important for heavily bombarded planetary surfaces, which

are likely to be composed of complex mineral assemblages rather than single components. We thus propose that shock effects may be an alternative interpretation for observed local shifts in metal–OH bands between 2.2 and 2.4 μm , and we suggest that reconsideration of some mineral-specific identifications may be warranted in future remote sensing investigations. Our results also demonstrate the importance of using multiple techniques (whenever possible) to specifically identify mineral species on remote planetary surfaces. The sensitivity of different remote and in situ sensing techniques to different parts of mineral structures makes comparisons between them particularly important when accounting for the effects of shock and other geologic processes on Mars. IR spectroscopy may not be sufficient to reveal the whole story of Martian mineralogy, but should be compared with other techniques, especially as we move closer to missions with sample return capabilities.

Our Mössbauer results in combination with the VNIR reflectance spectral results in the extended visible wavelength region demonstrate that shock changes the coordination polyhedra around the Fe^{3+} cations in nontronite, with site distortion increasing with shock pressure. Parameters of shocked samples must now be recognized to span a broad range of velocities, making unique mineral identifications very difficult. For example, jarosite ($\delta = 0.37$ mm/s and $\Delta = 1.20$ mm/s) [Morris *et al.*, 2006a] has identical parameters to nontronite shocked above 25.2 GPa ($\delta = 0.35$ mm/s and $\Delta = 1.19$ – 1.23 mm/s). Parameters cited for nanophase Fe oxide at Meridiani and in the Independence Class rocks of Clark *et al.* [2007] ($\delta = 0.33$ – 0.40 mm/s and $\Delta = 0.72$ – 1.16 mm/s) span the range of doublet parameters measured in this study from all shock pressures ($\delta = 0.33$ – 0.37 mm/s and $\Delta = 0.50$ – 0.75 mm/s). The problem here is that the range of possible Δ values in Fe^{3+} -bearing minerals is relatively small, and shock appears to cause even a single mineral to span a large portion of that possible range. If further experiments allow us to generalize this observation and we find that other clay (and silicate) minerals behave similarly, then it greatly complicates (and confuses) the assignment of specific Mössbauer features from the MERs. As with the effects on the VNIR and MIR spectra, an expanded range of parameters associated with shocked samples must now be considered when interpreting Martian remote and in situ sensing data. In addition, the association of MSL-identified phyllosilicates with X-ray amorphous materials [Bish *et al.*, 2013; Blake *et al.*, 2013; Morris *et al.*, 2014; Rampe *et al.*, 2014; Vaniman *et al.*, 2014] raises the possibility of mineral mixtures of altered and unaltered phyllosilicates (and other minerals) on the Martian surface. Although the formation mechanisms of these amorphous materials are not yet understood, impact processes should not be ruled out.

6. Conclusions

We provide a detailed spectroscopic analysis of the effects of experimental impacts and shock on the structure and spectra of a natural nontronite sample. Both VNIR and MIR spectra show increasing structural disorder with increasing pressure, eventually resembling hydrated amorphous silica (MIR) or an allophane-like phase (VNIR). At intermediate peak pressures, however, VNIR reflectance spectra may still be identified generally as Fe-rich smectite or nontronite. In contrast, MIR spectra much more closely resemble hydrated amorphous silicate phases. This is due to differences between the structural effects of shock on different parts of the nontronite mineral structure. In particular, MIR spectroscopy is sensitive to the more rapid total deformation of the tetrahedral sheet, while VNIR reflectance spectroscopy detects the retention of key features in the more structurally resilient octahedral sheet. TEM imaging, X-ray diffraction, Raman spectroscopy, and Mössbauer spectroscopy all confirm this increasing structural disorder and are consistent with observations implying that shock-induced structural change begins in the octahedral sheet but proceeds more quickly in the tetrahedral sheet.

Our findings provide important additional considerations for future planetary remote sensing and in situ analyses, although they significantly increase ambiguity and may limit our future ability to make mineral-specific identifications. However, our work does advance the ability to distinctly identify shocked versus unshocked nontronite, which may be important to furthering the current understanding of the geologic history of Mars. There are many potential future research directions that arise from our results. We recommend two, in particular. First, more laboratory spectroscopic investigations and analyses are needed to differentiate the spectral and structural effects of shock from the effects of thermal alteration, and to further explore variable effects of shock on different parts of the phyllosilicate structure. Second, detailed remote sensing investigations of heavily cratered regions of the Martian surface, particularly locations with strong VNIR phyllosilicate signatures and

absent MIR identifications, to look for the spectroscopic signatures of shocked clays may be an important extension of this research. We have already begun investigations of heavily cratered regions using impact-altered phyllosilicate laboratory VNIR spectra compared to well-described [Loizeau *et al.*, 2007] CRISM stamps using FATT and found that some phyllosilicate signatures at Mawrth Vallis are consistent with impact-induced spectral change [Friedlander and Glotch, 2014].

The results of this study build on previous work exploring both thermally and impact-altered phyllosilicates and demonstrate the importance of investigating shock effects in detail, both from the perspective of acquiring data over a range of pressures and with a wide variety of analytical techniques. We hypothesize that impacts may have altered the structures of Martian phyllosilicates, affecting their spectra in a way that explains the absence of MIR phyllosilicate identifications, even in regions with robust VNIR phyllosilicate spectral signatures.

Acknowledgments

This work was funded through a NASA Mars Fundamental Research Program grant to P. Joe Michalski (grant reference: NNX10AM83G). All of the referenced data from the VNIR reflectance, MIR emissivity, MIR ATR, and Raman spectroscopic results are available on the Stony Brook University Vibrational Spectroscopy Laboratory homepage (<http://aram.ess.sunysb.edu/tglotch/spectra.html>). Mössbauer results are available online through the Mount Holyoke Mars Mineral Spectroscopy database (<https://www.mtholyoke.edu/courses/mdyar/database/index.shtml?group=smect>). XRD and TEM data are available upon request by contacting Dave Bish (Bish@indiana.edu) and Tom Sharp (Tom.Sharp@asu.edu), respectively. Mark Cintala conducted impact experiments at the Flat Plate Accelerator facility at Johnson Space Center. The authors are particularly grateful for his expertise and assistance in providing essential information on the techniques used. The authors also wish to thank Patricia Craig and Janice Bishop for their detailed comments, which greatly improved the quality of this manuscript.

References

- Adams, J. B., F. Hörz, and R. V. Gibbons (1979), Effects of shock-loading on the reflectance spectra of plagioclase, pyroxene, and glass, in *Proc. Lunar and Planet. Sci. Conf. 10th*, pp. 5–7, Lunar and Planetary Institute, Houston, Tex.
- Altheide, T., V. Chevrier, and E. Noe Dobrea (2010), Mineralogical characterization of acid-weathered phyllosilicates with implications for secondary Martian deposits, *Geochim. Cosmochim. Acta*, *74*, 6232–6248.
- Analytical Spectral Devices (ASD) (2014), Incorporated website. [Available at <http://www.asdi.com/> (accessed November 13, 2014).]
- Bandfield, J. (2002), Global mineral distribution on Mars, *J. Geophys. Res.*, *107*(E6), 5042, doi:10.1029/2001JE001510.
- Bandfield, J. L., V. E. Hamilton, and P. R. Christensen (2000), A global view of Martian surface compositions from MGS-TES, *Science*, *287*, 1626–1630.
- Bibring, J., et al. (2005), Mars surface diversity as revealed by the OMEGA/Mars Express observations, *Science*, *307*(5715), 1576–1581.
- Bibring, J., et al. (2006), Global mineralogical and aqueous Mars history derived from OMEGA/Mars Express data, *Science*, *312*(5772), 400–404.
- Bischoff, A., and D. Stöffler (1992), Shock metamorphism as a fundamental process in the evolution of planetary bodies: Information from meteorites, *Eur. J. Mineral.*, *4*(4), 707–755.
- Bish, D. L., et al. (2013), X-ray diffraction results from Mars Science Laboratory: Mineralogy of Rocknest at Gale crater, *Science*, *341*(6153), doi:10.1126/science.1238932.
- Bishop, J., E. Murad, and M. D. Dyar (2002a), The influence of octahedral and tetrahedral cation substitution on the structure of smectites and serpentines as observed through infrared spectroscopy, *Clay Miner.*, *37*(4), 617–628, doi:10.1180/0009855023740064.
- Bishop, J., J. Madejová, P. Komadel, and H. Fröschl (2002b), The influence of structural Fe, Al and Mg on the infrared OH bands in spectra of dioctahedral smectites, *Clay Miner.*, *37*(4), 607–616, doi:10.1180/0009855023740063.
- Bishop, J., M. Lane, M. Dyar, and A. Brown (2008), Reflectance and emission spectroscopy study of four groups of phyllosilicates: Smectites, kaolinite-serpentines, chlorites and micas, *Clay Miner.*, *43*(1), 35–54.
- Bishop, J. L., and C. M. Pieters (1995), Low-temperature and low atmospheric pressure infrared reflectance spectroscopy of Mars soil analog materials, *J. Geophys. Res.*, *100*(E3), 5369, doi:10.1029/94JE03331.
- Bishop, J. L., and E. B. Rame (2014), The importance of nanophase aluminosilicates at Mawrth Vallis, *Proc. Lunar Planet. Sci. Conf. 45th*, Abstract 2068.
- Bishop, J. L., C. M. Pieters, and J. O. Edwards (1994), Infrared spectroscopic analyses on the nature of water in montmorillonite, *Clays Clay Miner.*, *42*(6), 702–716.
- Bishop, J. L., E. Murad, J. Madejová, P. Komadel, U. Wagner, and A. C. Scheinost (1999), Visible, Mössbauer and infrared spectroscopy of dioctahedral smectites: Structural analyses of the Fe-bearing smectites Sampor, SWY-1 and SWA-1, in *Proceedings of the 11th International Clay Conference, 1997*, pp. 413–419, The Clay Minerals Society, Bahia, Argentina.
- Bishop, J. L., P. Schifman, and R. Southard (2002c), Geochemical and mineralogical analyses of palagonitic tufts and altered rinds of pillow basalts in Iceland and applications to Mars, in *Volcano-Ice Interaction on Earth and Mars*, edited by J. L. Smellie and M. G. Chapman, pp. 371–392, Geol. Soc. of London, U. K.
- Blake, D. F., et al. (2013), Curiosity at Gale crater, Mars: Characterization and analysis of the Rocknest sand shadow, *Science*, *341*(6153), doi:10.1126/science.1239505.
- Boslough, M., E. Venturini, B. Morosin, R. Graham, and D. Williamson (1986), Physical properties of shocked and thermally altered nontronite: Implications for the Martian surface, *J. Geophys. Res.*, *91*(B13), E207–E214, doi:10.1029/JB091B13p0E207.
- Boslough, M. B., R. J. Weldon, and T. J. Ahrens (1980), Impact-induced water loss from serpentine, nontronite and kernite, *Proc. Lunar and Planet. Sci. Conf. 11th*, pp. 2145–2158, Lunar and Planetary Institute, Houston, Tex.
- Bougard, D., K. S. Smirnov, and E. Geidel (2000), Vibrational spectra and structure of kaolinite: A computer simulation study, *J. Phys. Chem. B*, *104*, 9210–9217.
- Bruckenthal, E. A., and C. M. Pieters (1984), Spectral effects of natural shock on plagioclase feldspar, *Proc. Lunar Planet. Sci. Conf. 15th*, pp. 96–97, Lunar and Planetary Institute, Houston, Tex.
- Burns, R. G. (1993), *Mineralogical Applications of Crystal Field Theory*, 2nd ed., Cambridge Univ. Press, New York.
- Butler, I., and R. Frost (2006), An overview of the high-pressure vibrational spectra of clays and related minerals, *Appl. Spectrosc. Rev.*, *41*(5), 449–471.
- Carroll, D. L., T. F. Kemp, T. J. Bastow, and M. E. Smith (2005), Solid-state NMR characterisation of the thermal transformation of a Hungarian white illite, *Solid State Nucl. Magn. Reson.*, *28*(1), 31–43, doi:10.1016/j.ssnmr.2005.04.001.
- Carter, J., F. Poulet, J.-P. Bibring, N. Mangold, and S. Murchie (2013), Hydrous minerals on Mars as seen by the CRISM and OMEGA imaging spectrometers: Updated global view, *J. Geophys. Res. Planets*, *118*, 831–858, doi:10.1029/2012JE004145.
- Chao, E. C. T., E. M. Shoemaker, and B. M. Madsen (1960), First natural occurrence of coesite, *Science*, *132*(3421), 220–222.
- Chao, E. C. T., J. J. Fahey, and J. Littler (1961), Coesite from Wabar Crater, near Al Hadida, Arabia, *Science*, *133*(3456), 882–883.
- Chao, E. C. T., J. J. Fahey, and J. Littler (1962), Stishovite, SiO₂, a very high pressure new mineral from Meteor Crater, Arizona, *J. Geophys. Res.*, *67*(1), 419–421, doi:10.1029/JZ067i001p00419.

- Che, C., and T. D. Glotch (2012), The effect of high temperatures on the mid-to-far-infrared emission and near-infrared reflectance spectra of phyllosilicates and natural zeolites: Implications for Martian exploration, *Icarus*, *218*(1), 585–601.
- Che, C., and T. D. Glotch (2014), Thermal alteration: A possible reason for the inconsistency between OMEGA/CRISM and TES detections of phyllosilicates on Mars?, *Geophys. Res. Lett.*, *41*, 321–327, doi:10.1002/2013GL058649.
- Che, C., T. Glotch, D. Bish, J. R. Michalski, and W. Xu (2011), Spectroscopic study of the dehydration and/or dehydroxylation of phyllosilicate and zeolite minerals, *J. Geophys. Res.*, *116*, E05007, doi:10.1029/2010JE003740.
- Chung, F. H. (1974), Quantitative interpretation of X-ray diffraction patterns of mixtures. II. Adiabatic principle of X-ray diffraction analysis of mixtures, *J. Appl. Crystallogr.*, *7*, 526–531, doi:10.1107/S0021889874010387.
- Clark, B. C., et al. (2007), Evidence for montmorillonite or its compositional equivalent in Columbia Hills, Mars, *J. Geophys. Res.*, *112*, E06S01, doi:10.1029/2006JE002756.
- Clark, R. N. (1999), Chapter 1: Spectroscopy of rocks and minerals, and principles of spectroscopy, in *Manual of Remote Sensing, Remote Sens. Earth Sci.*, vol. 3, edited by A. N. Rencz, pp. 3–58, John Wiley, New York.
- Clark, R. N., T. V. V. King, M. Klejwa, and G. A. Swayze (1990), High spectral resolution reflectance spectroscopy of minerals, *J. Geophys. Res.*, *95*(B8), 12,653–12,680, doi:10.1029/JB095iB08p12653.
- Coes, L. (1953), A new dense crystalline silica, *Science*, *118*(3057), 131–132.
- Craig, P. I., D. W. Ming, and E. B. Rampe (2014), Sulfate formation from acid-weathered phyllosilicates: Implications for the aqueous history of Mars, *Proc. Lunar Planet. Sci. Conf. 45th*, Abstract 1970.
- Daly, T., P. Gavin, and V. Chevrier (2011), Effects of thermal alteration on the near-infrared and mid-infrared spectra of Martian phyllosilicates, *Proc. Lunar Planet. Sci. Conf. 42nd*, Abstract 1164.
- De Carli, P. S., and D. J. Milton (1965), Stishovite: Synthesis by shock wave, *Science*, *147*(3654), 144–145.
- Dyar, M. D. (2002), Optical and Mössbauer spectroscopy of iron in micas, *Rev. Mineral. Geochem.*, *46*(1), 313–349.
- Dyar, M. D., D. G. Agresti, M. W. Schaefer, C. A. Grant, and E. C. Sklute (2006), Mössbauer spectroscopy of Earth and planetary materials, *Annu. Rev. Earth Planet. Sci.*, *34*(1), 83–125, doi:10.1146/annurev.earth.34.031405.125049.
- Dyar, M. D., M. W. Schaefer, E. C. Sklute, and J. L. Bishop (2008), Mössbauer spectroscopy of phyllosilicates: Effects of fitting models on recoil-free fractions and redox ratios, *Clay Miner.*, *43*(1), 3–33, doi:10.1180/claymin.2008.043.1.02.
- Ehlmann, B. L., J. F. Mustard, C. I. Fassett, S. C. Schon, J. W. Head III, D. J. Des Marais, J. A. Grant, and S. L. Murchie (2008), Clay minerals in delta deposits and organic preservation potential on Mars, *Nat. Geosci.*, *1*, 355–358.
- Ehlmann, B. L., et al. (2009), Identification of hydrated silicate minerals on Mars using MRO-CRISM: Geologic context near Nili Fossae and implications for aqueous alteration, *J. Geophys. Res.*, *114*, E00D08, doi:10.1029/2009JE003339.
- European Space Agency (2013), ESA: The ExoMars rover instrument suite. [Available at <http://exploration.esa.int/mars/45103-rover-instruments/> (Accessed 10 December 2013).]
- Fahrenfort, J. (1961), Attenuated total reflection: A new principle for the production of useful infra-red reflection spectra of organic compounds, *Spectrochim. Acta*, *17*(7), 698–709.
- Fairén, A. G., et al. (2010), Noachian and more recent phyllosilicates in impact craters on Mars, *Proc. Natl. Acad. Sci. U.S.A.*, *107*(27), 12,095–12,100, doi:10.1073/pnas.1002889107.
- Fitzgerald, J. J., A. I. Hamza, S. F. Dec, and C. E. Bronnimann (1996), Solid-state ²⁷Al and ²⁹Si NMR and ¹H CRAMPS studies of the thermal transformations of the 2:1 phyllosilicate pyrophyllite, *J. Phys. Chem.*, *3654*(96), 17,351–17,360.
- French, B. M. (1968), Shock metamorphism as a geologic process, in *Shock Metamorphism of Natural Materials: Proceedings of the First Conference Held at NASA, Goddard Space Flight Center, Greenbelt, Maryland, April 14–16, 1966*, edited by B. M. French and N. M. Short, pp. 1–17, Mono Book Corp, Baltimore, Md.
- French, B. M. (1998), *Traces of Catastrophe: A Handbook of Shock-Metamorphic Effects in Terrestrial Meteorite Impact Structures*, LPI Contributions, Lunar and Planetary Institute, Houston, Tex.
- Friedlander, L. R., and T. D. Glotch (2014), Phyllosilicate spectra identified at Mawrth Vallis by factor analysis and target transformation are consistent with impact-related spectral change, *Proc. Lunar Planet. Sci. Conf. 45th*, Abstract 2001.
- Friedlander, L. R., T. Glotch, J. R. Michalski, T. G. Sharp, M. D. Dyar, and D. L. Bish (2012), Spectroscopic studies of nontronite after impacts at 3 pressures, *Proc. Lunar Planet. Sci. Conf. 43rd*, Abstract 2520.
- Frost, R. L. (1995), Fourier transform Raman spectroscopy of kaolinite, dickite and halloysite, *Clays Clay Miner.*, *43*(2), 191–195.
- Frost, R. L., and J. T. Kloprogge (2000), Vibrational spectroscopy of ferruginous smectite and nontronite, *Spectrochim. Acta, Part A*, *56*, 2177–2189.
- Frost, R. L., J. T. Kloprogge, and D. Zhe (2002), The Garfield and Uley nontronites—an infrared spectroscopic comparison, *Spectrochim. Acta, Part A*, *58*, 1881–1894.
- Gault, D. E., and E. D. Heitowitz (1963), The partition of energy for hypervelocity impact craters formed in rock, in *Proceedings of the 6th Hypervelocity Impact Symposium*, pp. 1–38, National Aeronautics and Space Administration, Cleveland, Ohio/Moffett Field, Calif.
- Gavin, P., and V. Chevrier (2010), Thermal alteration of nontronite and montmorillonite: Implications for the Martian surface, *Icarus*, *208*(2), 721–734, doi:10.1016/j.icarus.2010.02.027.
- Gavin, P., V. Chevrier, K. Ninagawa, A. Gucsik, and S. Hasegawa (2009), Experimental investigation of the effect of meteoritic impacts on clays on Mars, *Proc. Lunar Planet. Sci. Conf. 40th*, Abstract 2069.
- Gavin, P., V. Chevrier, K. Ninagawa, A. Gucsik, and S. Hasagawa (2013), Experimental investigation into the effects of meteoritic impacts on the spectral properties of phyllosilicates on Mars, *J. Geophys. Res.*, *118*, 1–16, doi:10.1029/2012JE004185.
- Gibbons, R. V., and T. J. Ahrens (1971), Shock metamorphism of silicate glasses, *J. Geophys. Res.*, *76*(23), 5489–5498, doi:10.1029/JB076i023p05489.
- Hans, R. E., M. K. Montague, C. Davis, and C. Galindo (1978), X-ray diffractometer studies of shocked materials, *Proc. Lunar Planet. Sci. Conf. 9th*, pp. 2773–2787, Lunar and Planetary Institute, Houston, Tex.
- Harris, W. G., K. A. Hollien, S. R. Bates, and W. A. Acree (1992), Dehydration of hydroxy-interlayered vermiculite as a function of time and temperature, *Clays Clay Miner.*, *40*(3), 335–340, doi:10.1346/CCMN.1992.0400314.
- Haynes, W. M., and D. R. Lide (Eds.) (2010), *CRC Handbook of Chemistry and Physics*, 90th ed. (internet version), CRC Press/Taylor and Francis, Boca Raton, Fla.
- Huang, E., A. Li, J. Xu, R. Chen, and T. Yamanaka (1996), High-pressure phase transition in Al(OH)₃: Raman and X-ray observations, *Geophys. Res. Lett.*, *23*(22), 3083–3086, doi:10.1029/96GL03023.
- Huang, Y., Z. Jiang, and W. Schwieger (1999), Vibrational spectroscopic studies of layered silicates, *Chem. Mater.*, *11*, 1210–1217.
- Hugoniot, H. (1889), Sur la propagation du mouvement dans les corps et spécialement dans les gaz parfaits, *J. Ec. Polytech.*, *58*, 1–125.
- Johnson, J. R., and F. Hörz (2003), Visible/near-infrared spectra of experimentally shocked plagioclase feldspars, *J. Geophys. Res.*, *108*(E11), 5120, doi:10.1029/2003JE002127.

- Johnson, J., F. Hörs, P. G. Lucey, and P. R. Christensen (2002), Thermal infrared spectroscopy of experimentally shocked anorthosite and pyroxenite: Implications for remote sensing of Mars, *J. Geophys. Res.*, *107*(E10), 5073, doi:10.1029/2001JE001517.
- Johnson, J. R., M. I. Staid, and M. D. Kraft (2007), Thermal infrared spectroscopy and modeling of experimentally shocked basalts, *Am. Mineral.*, *92*(7), 1148–1157, doi:10.2138/am.2007.2356.
- Keeling, J. L., M. D. Raven, and W. P. Gates (2000), Geology and characterization of two hydrothermal nontronites from weathered metamorphic rocks at the Uley graphite mine, South Australia, *Clays Clay Miner.*, *48*(5), 537–548.
- Kraus, R. G., S. T. Stewart, M. G. Newman, R. E. Milliken, and N. J. Tosca (2013), Uncertainties in the shock devolatilization of hydrated minerals: A nontronite case study, *J. Geophys. Res. Planets*, *118*, 2137–2145, doi:10.1002/jgre.20147.
- Lange, M. A., and T. J. Ahrens (1982), Impact induced dehydration of serpentine and the evolution of planetary atmospheres, *J. Geophys. Res.*, *87*(Supplement), A451–A456, doi:10.1029/JB087iS01p0A451.
- Liu, Y., and T. Glotch (2014), Spectral mixture analysis of hydrated minerals in southwest Melas Chasma, *Proc. Lunar Planet. Sci. Conf. 45th*, Abstract 2443.
- Loizeau, D., et al. (2007), Phyllosilicates in the Mawrth Vallis region of Mars, *J. Geophys. Res.*, *112*, E08S08, doi:10.1029/2006JE002877.
- Mangold, N., et al. (2007), Mineralogy of the Nili Fossae region with OMEGA/Mars Express data: 2. Aqueous alteration of the crust, *J. Geophys. Res.*, *112*, E08S04, doi:10.1029/2006JE002835.
- McDowell, M., and V. Hamilton (2009), Seeking phyllosilicates in thermal infrared data: A laboratory and Martian data case study, *J. Geophys. Res.*, *114*, E06007, doi:10.1029/2008JE003317.
- Mckeown, N., J. Bishop, E. Noe Dobrea, B. Ehlmann, M. Parente, J. Mustard, S. Murchie, G. Swayze, J. Bibring, and E. Silver (2009), Characterization of phyllosilicates observed in the central Mawrth Vallis region, Mars, their potential formational processes, and implications for past climate, *J. Geophys. Res.*, *114*, E00D10, doi:10.1029/2008JE003301.
- Michalski, J., M. Kraft, T. Sharp, L. Williams, and P. Christensen (2006), Emission spectroscopy of clay minerals and evidence for poorly crystalline aluminosilicates on Mars from Thermal Emission Spectrometer data, *J. Geophys. Res.*, *111*, E03004, doi:10.1029/2005JE002438.
- Michalski, J., F. Poulet, J.-P. Bibring, and N. Mangold (2010), Analysis of phyllosilicate deposits in the Nili Fossae region of Mars: Comparison of TES and OMEGA data, *Icarus*, *206*(1), 269–289, doi:10.1016/j.icarus.2009.09.006.
- Michalski, J. R., and E. Z. N. Dobrea (2007), Evidence for a sedimentary origin of clay minerals in the Mawrth Vallis region, Mars, *Geology*, *35*(10), 951, doi:10.1130/G23854A.1.
- Michalski, J. R., and R. L. Fergason (2008), Composition and thermal inertia of the Mawrth Vallis region of Mars from TES and THEMIS data, *Icarus*, *199*(1), 25–48.
- Michalski, J. R., M. D. Kraft, T. G. Sharp, L. B. Williams, and P. R. Christensen (2005), Mineralogical constraints on the high-silica Martian surface component observed by TES, *Icarus*, *174*(1), 161–177, doi:10.1016/j.icarus.2004.10.022.
- Milliken, R. E. (2014), Widespread diagenesis on Mars and implications for crustal fluids, in *Proceedings of the 8th International Conference on Mars*, Abstract 1253.
- Moore, D. M., and R. C. J. Reynolds (1989), X-ray diffraction and the identification and analysis of clay minerals, in *X-Ray Diffraction and the Identification and Analysis of Clay Minerals*, pp. 187–190, Oxford Univ. Press, Oxford U. K.
- Morris, R. V., et al. (1985), Spectral and other physicochemical properties of submicron powders of hematite (α -Fe₂O₃), maghemite (γ -Fe₂O₃), magnetite (Fe₃O₄), goethite (α -FeOOH), and lepidocrocite (γ -FeOOH), *J. Geophys. Res.*, *90*(B4), 3126–3144, doi:10.1029/JB090iB04p03126.
- Morris, R. V., et al. (2006a), Mössbauer mineralogy of rock, soil, and dust at Gusev crater, Mars: Spirit's journey through weakly altered olivine basalt on the plains and pervasively altered basalt in the Columbia Hills, *J. Geophys. Res.*, *111*, E02S13, doi:10.1029/2005JE002584.
- Morris, R. V., et al. (2006b), Mössbauer mineralogy of rock, soil, and dust at Meridiani Planum, Mars: Opportunity's journey across sulfate-rich outcrop, basaltic sand and dust, and hematite lag deposits, *J. Geophys. Res.*, *111*, E12S15, doi:10.1029/2006JE002791.
- Morris, R. V., et al. (2009), Visible and near-IR reflectance spectra for smectite, sulfate and perchlorate under dry conditions for interpretation of Martian surface mineralogy, *Proc. Lunar Planet. Sci. Conf. 40th*, Abstract 2317.
- Morris, R. V., et al. (2010), Evidence for interlayer collapse of nontronite on Mars from laboratory visible and near-IR reflectance spectra, *Proc. Lunar Planet. Sci. Conf. 41st*, Abstract 2156.
- Morris, R. V., et al. (2011), Visible and near-IR reflectance spectra of Mars-analogue materials under arid conditions for interpretation of Martian surface mineralogy, *Proc. Lunar Planet. Sci. Conf. 42nd*, Abstract 2757.
- Morris, R. V., et al. (2014), Chemical composition of crystalline, smectite, and amorphous components for Rocknest soil and John Klein and Cumberland mudstone drill fines using APXS, ChemMin, and SAM datasets from Gale Crater, Mars, *Proc. Lunar Planet. Sci. Conf. 45th*, Abstract 1319.
- Moskowitz, B., and R. Hargraves (1984), Magnetic cristobalite? A possible new magnetic phase produced by the thermal decomposition of nontronite, *Science*, *255*(4667), 1152–1154.
- Music, S., N. Filipovic-Vincekovic, and L. Sekovanic (2011), Precipitation of amorphous SiO₂ particles and their properties, *Brazilian J. Chem. Eng.*, *28*(01), 89–94.
- Mustard, J. F., et al. (2008), Hydrated silicate minerals on Mars observed by the Mars Reconnaissance Orbiter CRISM instrument, *Nature*, *454*(7202), 305–309, doi:10.1038/nature07097.
- Mustard, J. F., et al. (2013), Report of the Mars 2020 science definition team. [Available at http://mepag.jpl.nasa.gov/reports/MEP/Mars_2020_SDT_Report_Final.pdf]
- Neumann, A., S. Petit, and T. Hofstetter (2011), Evaluation of redox-active iron sites in smectites using middle and near infrared spectroscopy, *Geochim. Cosmochim. Acta*, *75*, 2336–2355.
- Ohashi, F., S.-I. Wada, M. Suzuki, M. Maeda, and S. Tomura (2002), Synthetic allophane from high-concentration solutions: Nanoengineering of the porous solid, *Clay Miner.*, *37*(3), 451–456, doi:10.1180/0009855023730052.
- Palin, E. J., and M. T. Dove (2004), Investigation of Al/Si ordering in tetrahedral phyllosilicate sheets by Monte Carlo simulation, *Am. Mineral.*, *89*, 176–184.
- Pelkey, S. M., et al. (2007), CRISM multispectral summary products: Parameterizing mineral diversity on Mars from reflectance, *J. Geophys. Res.*, *112*, E08S14, doi:10.1029/2006JE002831.
- Petit, S., J. Madejova, A. Decarreau, and F. Martin (1999), Characterization of octahedral substitutions in kaolinites using near infrared spectroscopy, *Clays Clay Miner.*, *47*(1), 103–108.
- Petit, S., J. Caillaud, D. Righi, J. Madejová, F. Elsass, and H. Köster (2002), Characterization and crystal chemistry of an Fe-rich montmorillonite from Ölberg, Germany, *Clay Miner.*, *37*(2), 283–297.
- Petit, S., A. Decarreau, F. Martin, and R. Buchet (2004), Refined relationship between the position of the fundamental OH stretching and the first overtones for clays, *Phys. Chem. Miner.*, *31*(9), 585–592.
- Poulet, F. (2004), Nonlinear spectral mixing: Quantitative analysis of laboratory mineral mixtures, *J. Geophys. Res.*, *109*, E02009, doi:10.1029/2003JE002179.

- Poulet, F., et al. (2005), Phyllosilicates on Mars and implications for early Martian climate, *Nature*, 438(7068), 623–627.
- Poulet, F., N. Mangold, D. Loizeau, J. Bibring, Y. Langevin, J. Michalski, and B. Gondet (2008), Abundance of minerals in the phyllosilicate-rich units on Mars, *Astron. Astrophys.*, 487(2), L41–L44.
- Poulet, F., D. Beaty, J. Bibring, D. Bish, J. Bishop, E. Dobreá, J. Mustard, S. Petit, and L. Roach (2009), Key scientific questions and key investigations from the first international conference on Martian phyllosilicates, *Astrobiology*, 9(3), 257–267.
- Raikes, S. A., and T. J. Ahrens (1979), Measurements of post-shock temperatures in aluminum and stainless steel, in *High Pressure Science and Technology*, vol. 2, edited by K. D. Timmerhaus and M. S. Barber, pp. 889–894, Plenum Press, New York.
- Rampe, E. B., et al. (2012), Allophane detection on Mars with thermal emission spectrometer data and implications for regional-scale chemical weathering processes, *Geology*, 40(11), 995–998.
- Rampe, E. B., et al. (2014), Characterizing the phyllosilicate component of the Sheepbed mudstone in Gale Crater, Mars using laboratory XRD and EGA, *Proc. Lunar Planet. Sci. Conf. 45th*, Abstract 2068.
- Rankine, W. J. M. (1870), On the thermodynamic theory of waves of finite longitudinal disturbance, *Proc. R. Soc. London*, 18, 80–83.
- Roch, G. E., M. E. Smith, and S. R. Drachman (1998), Solid state NMR characterization of the thermal transformation of an illite-rich clay, *Clays Clay Miner.*, 46(6), 694–704.
- Rocha, J. (1999), Single- and triple-quantum ^{27}Al MAS NMR study of the thermal transformation of kaolinite, *J. Phys. Chem. B*, 103, 9801–9804.
- Rouff, A., B. L. Phillips, S. G. Cochiara, and K. L. Nagy (2012), The effect of dissolved humic acids on aluminosilicate formation and associated carbon sequestration, *Appl. Environ. Sci.*, doi:10.1155/2012/430354.
- Ruff, S. (2003), Basaltic andesite or weathered basalt: A new assessment, *Sixth Int. Conf. Mars*, Abstract 3258, Pasadena, Calif.
- Ruff, S., and P. Christensen (2007), Basaltic andesite, altered basalt, and a TES-based search for smectite clay minerals on Mars, *Geophys. Res. Lett.*, 34, L10204, doi:10.1029/2007GL029602.
- Ruff, S., and V. Hamilton (2009), New insights into the nature of mineralogic alteration on Mars from orbiter, rover, and laboratory data, *Proc. Lunar Planet. Sci. Conf. 40th*, Abstract 2160.
- Ruff, S. W., P. R. Christensen, P. W. Barbera, and D. L. Anderson (1997), Quantitative thermal emission spectroscopy of minerals: A laboratory technique for measurement and calibration, *J. Geophys. Res.*, 102(B7), 14,899–14,913, doi:10.1029/97JB00593.
- See, T. H., F. Cardenas, and R. Montes (2012), The Johnson Space Center Experimental Impact Lab: Contributions toward understanding the evolution of the solar system, *Proc. Lunar Planet. Sci. Conf. 43rd*, Abstract 2488.
- Sharp, T. G., J. R. Michalski, M. D. Dyar, D. L. Bish, L. R. Friedlander, and T. Glotch (2012), Effects of shock metamorphism on phyllosilicate structures and spectroscopy, *Proc. Lunar Planet. Sci. Conf. 43rd*, Abstract 2806.
- Skogby, H., H. Annersten, M. C. Domeneghetti, G. M. Molin, and V. Tazzoli (1992), Iron distribution in orthopyroxene: A comparison of Mössbauer spectroscopy and X-ray refinement results, *Eur. J. Mineral.*, 4, 441–452.
- Stishov, S. M., and S. V. Popova (1961), A new modification of silica, *Geokhimiya*, 10, 923–926.
- Stöffler, D. (1971), Coesite and stishovite in shocked crystalline rocks, *J. Geophys. Res.*, 76(23), 5474–5488, doi:10.1029/JB076i023p05474.
- Stöffler, D. (1972), Deformation and transformation of rock-forming minerals by natural and experimental shock processes: I. Behavior of minerals under shock compression, *Fortschritte der Mineral.*, 49(197), 50–113.
- Stöffler, D. (1974), Deformation and transformation of rock-forming minerals by natural and experimental shock processes: II. Physical properties of shocked minerals, *Fortschritte der Mineral.*, 51, 256–289.
- Stöffler, D. (1984), Glasses formed by hypervelocity impact, *J. Non Cryst. Solids*, 67(1–3), 465–502.
- Tarte, P., A. Rulmont, M. Liégeois-Duyckaerts, R. Cahay, and J. M. Winand (1990), Vibrational spectroscopy and solid state chemistry, *Solid State Ionics*, 42, 177–196.
- Thomas, N. H., and J. Bandfield (2013), Identification of spectral end members in CRISM data using factor analysis and target transformation, *Proc. Lunar Planet. Sci. Conf. 44th*, Abstract 1325.
- Tyburczy, J. A., and T. J. Ahrens (1987), Dehydration kinetics of shocked serpentine, *Proc. Lunar Planet. Sci. Conf. 18th*, pp. 435–441, Cambridge Univ. Press/Lunar and Planetary Institute, Cambridge and New York/Houston, Tex.
- Vaniman, D. T., et al. (2014), Mineralogy of a mudstone at Yellowknife Bay, Gale crater, Mars, *Science*, 343(6169), doi:10.1126/science.1243480.
- Viviano, C. E., and J. E. Moersch (2012), A technique for mapping Fe/Mg-rich phyllosilicates on Mars using THEMIS multispectral thermal infrared images, *J. Geophys. Res.*, 117, E07007, doi:10.1029/2011JE003985.
- Weldon, R. J., W. M. Thomas, M. B. Boslough, and T. J. Ahrens (1982), Shock-induced color changes in nontronite: Implications for the Martian fines, *J. Geophys. Res.*, 87(B12), 10,102–10,114, doi:10.1029/JB087iB12p10102.
- Wray, J., E. Noe Dobreá, R. Arvidson, S. Wiseman, S. Squyres, A. Mcewen, J. Mustard, and S. Murchie (2009), Phyllosilicates and sulfates at Endeavour Crater, Meridiani Planum, Mars, *Geophys. Res. Lett.*, 36, L21201, doi:10.1029/2009GL040734.
- Wright, S. P., P. R. Christensen, and T. G. Sharp (2006), Thermal emission spectroscopy of shocked basalt from the Earth and Mars: A review plus new insights, *Proc. Lunar Planet. Sci. Conf. 37th*, Abstract 1786.
- Wyatt, M., and H. McSween (2002), Spectral evidence for weathered basalt as an alternative to andesite in the northern lowlands of Mars, *Nature*, 417(6886), 263–266.